Introduction

Rubber-like materials are extensively used in industrial applications because of their ability to undergo large deformations and of their damping behaviour. Elastomeric components used in the automotive industry, such as engine mounts or torque rod, are submitted to cyclic loadings and a good conception towards fatigue phenomenon is therefore mandatory to ensure the safety of these structures. Fatigue initiation properties are studied by submitting specimens of a given geometry to a given cyclic load and measuring the number of cycles needed to reach an end-of-life criterion (presence of a crack of a given length, fracture of the specimen or stiffness loss). From these results, the so-called Wöhler curve, or "S/N" curve (Stress or Strain vs Number of cycles) is built. To be reliable, this classical method presents at least two main disadvantages: it requires long duration tests and a large number of specimens (usually a minimum of 25 specimens is required) in order to have a good estimation of the fatigue intrinsic dispersion. These two disadvantages obviously limit the study of fatigue properties and the determination of the influences of some parameters (*i.e.* mean load, amplitude load, etc.) on these properties. To reduce this cost (of time and money), other methods have to be developed.

For several years, different methods for the rapid estimation of mean fatigue limits of metallic materials, based on temperature measurements, have been developed (see [2] and references therein). The aim of this paper is to investigate the opportunity to use these methods for rubber-like materials. In a first part, a heat build-up experiment and the associated analysis suitable for metallic materials is reminded. Based on this protocol, a heat build-up experiment suitable for rubber-like materials is proposed in a second part. Taking into account the specific aspects of this kind of materials, the experiment links the temperature rise to the principal maximum strain. In a third part, the relevance of a link between thermal measurements and fatigue properties is discussed from the results obtained on fifteen industrial materials. Even if this empirical approach gave some interesting results, it was also observed that, as expected, the viscosity has a first order influence on the temperature rise. It was therefore difficult to identify the dissipated energy only related to the fatigue mechanisms. These fatigue mechanisms are strongly linked to the flaw population and to the cavities created along a fatigue test. In a forth part we consequently use the microstructural informations obtained from a X-ray computed micro-tomography investigation [1] to evaluate the ratio of the global dissipated energy to the one related to

the fatigue damage. A critical energy criterion is applied and the results are compared to a Wöhler curve obtained classically. This comparison exhibits a very good correlation, opening a very promising field of investigation.

1. Material and testing

1.1. Material and specimens

A wide range of elastomeric materials, based on industrial standard recipes, are used in this study. The aim was to cover a wide range of materials, crystallizing, non crystallizing, unfilled, monomer or copolymers matrix with a wide range of mechanical properties (fatigue lifetime, $\tan\delta$). More than 15 materials were tested. Hourglass shaped specimens were manufactured from a single batch in order to ensure the reliability of mixing and moulding conditions. The geometry of the specimen is given on figure 1. This kind of specimen (called AE2 in the following) was chosen for several reasons:

- it is classically used to obtain Wöhler curves;
- the initiation and break zone is well controlled and is located in the thinner section (no cracks location in the massive zones neither at the bounding between the metallic inserts and the rubber, in the contrary to more massive "diabolo" samples or samples submitted to heavy shear loads);
- the central section is thin enough to prevent a high temperature gradient between the skin and the core due the low thermal conductibility of rubber.

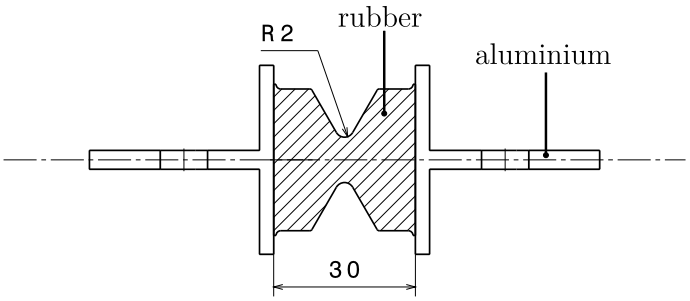

Figure 1: AE2 specimen

1.2. Heat build-up based protocol for metallic materials

For several years, different methods for the rapid estimation of mean fatigue limits of metallic materials based on temperature measurements have been developed [2]. They consist in applying successive sets of a given number of cycles for different increasing stress levels (figure 2(a)). For each

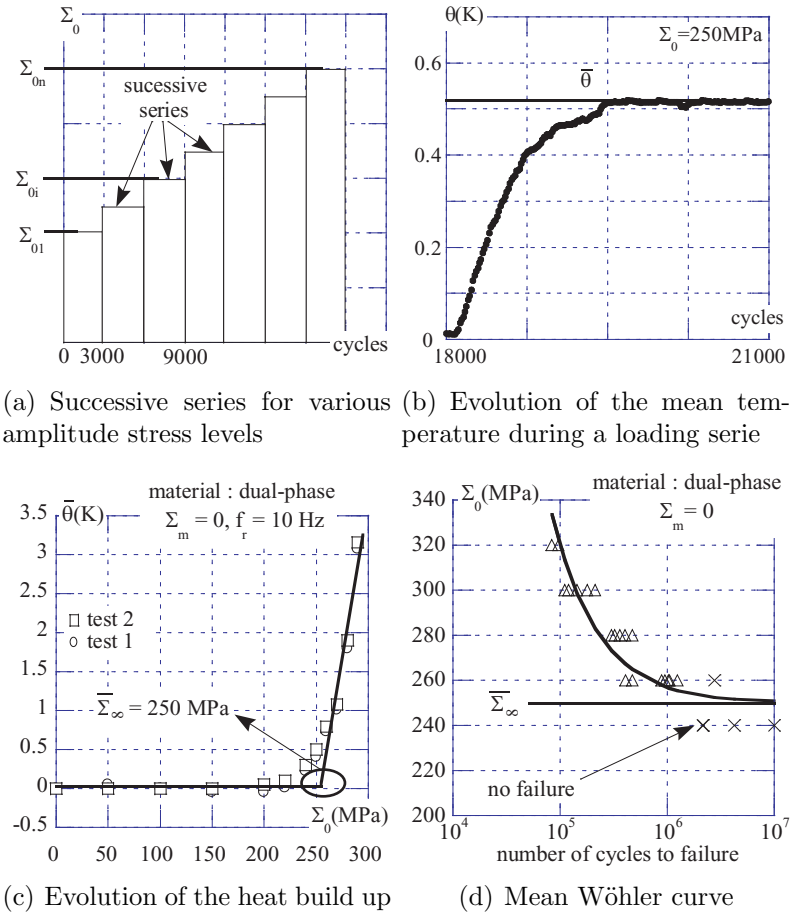

(a) Successive series for various amplitude stress levels

(b) Evolution of the mean temperature during a loading serie

(c) Evolution of the heat build up

(d) Mean Wöhler curve

Figure 2: Empirical method to correlate heat build-up measurements to mean fatigue duration [2].

stress level, the change of the temperature difference $\theta = T - \frac{T_1+T_2}{2}$ (where T is the current temperature of the sample during the test measured by a thermocouple or an infrared camera, T_1 and T_2 are the current temperatures of the lower and upper grips) is recorded and the steady-state temperature $\bar{\theta}$ is determined (figure 2(b)). Beyond a given limit it is observed that the

steady-state temperature starts to increase significantly (figure 2(c)). This change is correlated with a state where the fatigue limit is exceeded and can be related to the apparition of microplasticity, *i.e.* plasticity at a microscopic scale, which occurrs in the material and governs the fatigue properties. A correlation between the mean fatigue limit and the heat build-up is illustrated on figures 2(c) and 2(d) [3]. More recently, the development of a two-scale probabilistic model has shown that heat build-up tests permit to identify not only the mean fatigue limit but also the scatter of classical fatigue results. Indeed, by using the two-scale probabilistic model and an energetic criterion based on a constant critical dissipated energy, it is possible to predict the S/N curves for any given probability of failure using a single specimen in less than half a day [2].

1.3. Measurement protocol developed for rubber-like materials

1.3.1. Temperature measurement

A heat build-up experiment can be defined as a succession of cyclic tests of increasing loading conditions during which the temperature of the specimen is measured. The number of cycles used for each loading condition is the number of cycles needed for the temperature to stabilize (for example, 2000 cycles at 2 Hz are sufficient for rubber-like materials). For the temperature measurement, we were facing two major technical problems: we have to set up an experiment that takes into account the large displacements of the specimen during a fatigue test and to properly define a heat build-up temperature. The responses to these problems were depending on the technological solution we retain for the temperature measurements. The use of thermocouples is possible but it presents some technological limitations (fixation on the specimen, response time of about 1 s for classical thermocouples) and the main point is that it only gives a local information. We have chosen to use an infrared camera, which gives access to a 2D measurement with a high acquisition rate (50 frames/seconds) and a very good precision (about 30 mK), even if it will only be a surface measurement. However, AE2 specimen are thinner enough to avoid a too high core/skin temperature ratio.

The infrared camera that has been used is a Flir Systems camera (reference Phoenix MWIR 9705) with a Stirling-cycle cooled Indium Antimonide (InSb) Focal Plane Array (FPA). The FPA is a 320×256 array of detectors digitized on 14 bits, sensitive in the 3 μm-5 μm spectral band. A preliminary calibration operation allows the conversion of the thermosignal (pro-

portional to the thermal radiation) into a temperature in Celcius degree (°C).

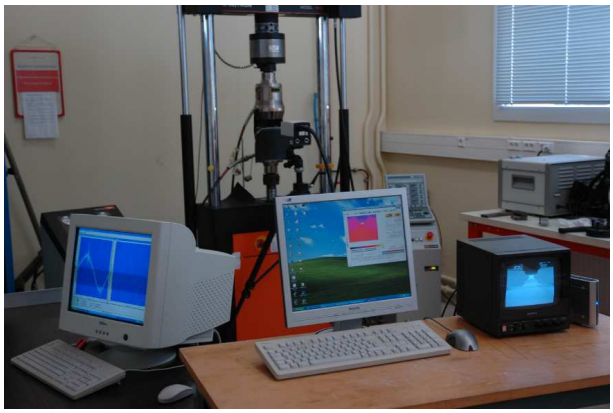

Figure 3: Experimental set-up.

Figure 4 presents one example of temperature evolution of the central zone of the specimen during cyclic solicitation (20 cycles). We can note

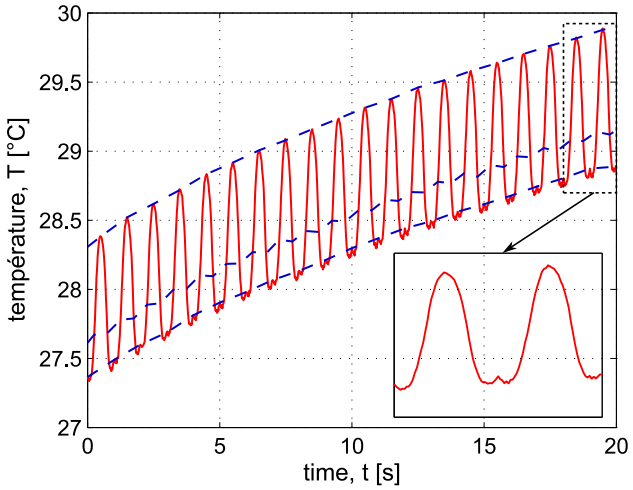

Figure 4: Evolution of the temperature of the central zone of the specimen during cyclic solicitation measured with an infrared camera ($R = 0\,@\,1\,\mathrm{Hz}$, maximum displacement: 10 mm). The dotted lines relate to the temperatures measured in the non-deformed, mid-deformed and deformed positions.

a mean rise of the temperature due to an intrinsic dissipation and an oscillation of the temperature during one cycle which is caused by the thermomechanical couplings (mainly thermoelastic effects). The amplitude of

these coupling effects could attain one Celsius degree. We consequently had to make sure that the temperature is measured for a *given position* of the specimen to define accurately a heat build-up temperature. We used here sequences of movies (performed at an acquisition frequency of 50 Hz), which allowed the evaluation of the temperature during one movie for any deformation of the sample (figure 5). For simplicity reasons and because all experiments are carried out at a loading ratio $R = 0$, we have chosen to retain only temperatures associated to the non deformed (fig. 5(b)) and maximum deformed position (fig. 5(c)) of the specimen during one loading cycle. We should remark that the temperatures associated to these posi-

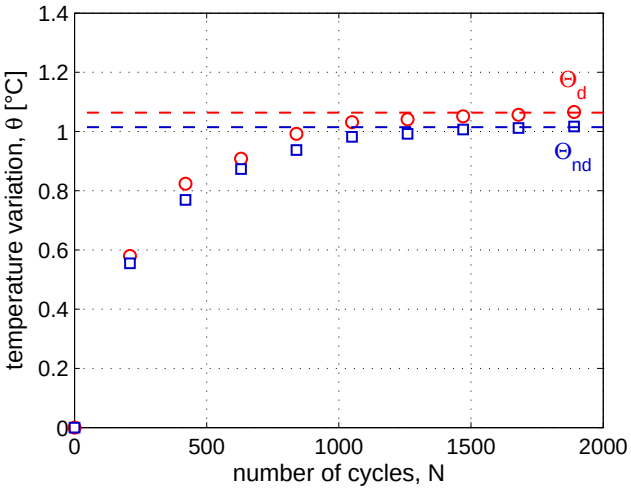

(a) Evolution of the temperature variation

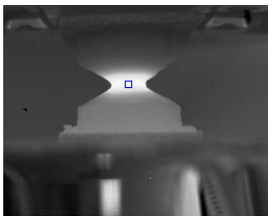

(b) non deformed position

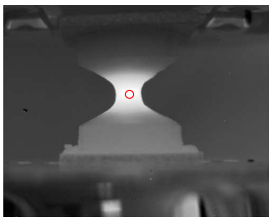

(c) maximum deformed position

Figure 5: Evolution of the temperature variation envelope for a value of displacement amplitude of 0.6 mm.

tions are not necessarily the minimum and maximum temperatures reached during one cycle because of the thermoelastic inversion phenomenon which

can be clearly seen on figure 4 [4–6].

For each loading block, we get an envelope of temperature (figure 5(a)) and we evaluate the amplitude of the thermomechanical coupling effects (difference between the temperatures measured in the maximum deformed position and non-deformed position). The temperature variation is calculated from the current temperature T and the initial temperature T_0 using the equation $\theta = T - T_0$ and the steady-state temperatures Θ_{nd} (related to the non deformed position) and Θ_d (related to the maximum deformed position) are determined according to the processing presented on figure 5(a). To take into account the global heating of the machine test, the temperature gradient of the specimen and the low thermal conductivity of rubber-like materials, a pause of 15 min is performed at the end of each loading block in order to ensure the temperature stabilization and homogeneity.

1.3.2. Heat build-up curve construction

Based on the successive loads carried out on an AE2 specimen, we can generate a heat build-up curve by associating a fatigue predictor (for fatigue crack nucleation) with the steady-state temperatures. There is no universally used predictor in the literature. As the tests were displacement controlled, we chose the maximum principal strain ε_{max} which is one of the most commonly used [7–9] and which has been proven to be relevant for the AE2 specimen [9]. A heat build-up curve is therefore plotted from the steady-state temperatures as a function of ε_{max} as illustrated on figure 6.

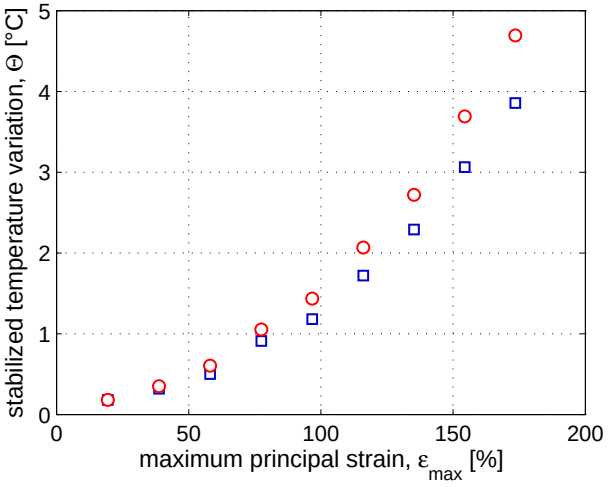

Figure 6: Heat build-up curve example.

1.4. Mechanical testing

All heat build-up tests were performed on a servo-hydraulic test machine (Instron 1342) at a frequency of 2 Hz and were dispacement controlled. This frequency was chosen to be the same than the one used to perform the fatigue tests, in order to be as representative as possible from the fatigue lifetime evaluation. In order to evaluate the influence of this important testing parameter on the temperature rise, we performed a few tests with several frequencies, which lead to highlight a linear dependency of the stabilised temperature reached with the testing frequency. The fatigue tests were performed at Trelleborg-Modyn laboratory on machines that have already been described elsewhere [10]. The experimental determination of the initiation Wöhler curve was achieved using a end-of-life criterion based on the variation of the effective stiffness proposed by [10]. It has been shown that the criterion is equivalent to the apparition of crack of 2 mm on the surface of the specimen [9].

1.5. Tan δ measurements

Tan δ is an indicator of the viscous potential of a material. Its value is not an intrinsic characteristic of a material but depends on the loading conditions. Consequently, it is very important to mention the test conditions related to the value of $\tan\delta$ that are used. All measurements are performed on compression specimens (diameter: 29 mm and height: 12 mm). A static compression strain of 10% is applied and the dynamic load condition is a strain amplitude of 0.5% at 2 Hz. The $\tan\delta$ value is then computed from the stress-strain response.

2. Results and discussion on the thermal measurements

2.1. First observations

In this paper, up to fifteen industrial materials have been tested. It was therefore mandatory to evaluate if the tests were repeatable in order to ensure the reliability of the differences between the different materials. This requirement was checked for several materials tested with small variations of the ambient temperature and for different loading histories (different numbers of loading blocks, with different increasing amplitudes). Figure 7 illustrates well that the heat build-up tests gave the same curves for these different testing conditions.

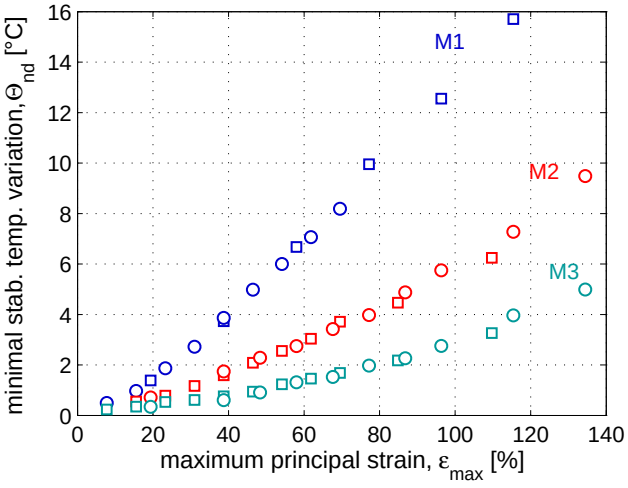

Figure 7: Comparison for three materials (referenced as M1, M2 and M3) of the heat build-up curves of two different specimens submitted to different loading conditions. For legibility reasons, only the temperatures associated to the non-deformed positions of the specimens are plotted.

2.2. A direct link with fatigue?

At this stage of the study, we were evaluating if a quick empirical protocol similar to the one used for metallic materials could be used. In order to take into account several kinds of material and different thermo-mechanical properties, a wide range of materials was investigated (more than fifteen industrial materials were tested). We followed here a threefold approach:

- identify an empirical protocol giving the maximum strain leading to a damage initiation after 10^6 cycles for a given material;
- apply this protocol on several materials in order to test its validity;
- investigate its sensitivity to the material viscosity.

Figure 8 presents the temperature measurements obtained for material G (cf. table 1) and a proposal of empirical analysis, similar to the one proposed for metallic materials. The material G was chosen because it presents a $\tan\delta$ of average value. As the fatigue mechanisms are dissipative, we used only the rise of temperature corresponding to the dissipative sources (square symbols on figure 6), excluding the thermo-elastic contribution. One can see that the evolution of the heat build-up curve is much smoother than for

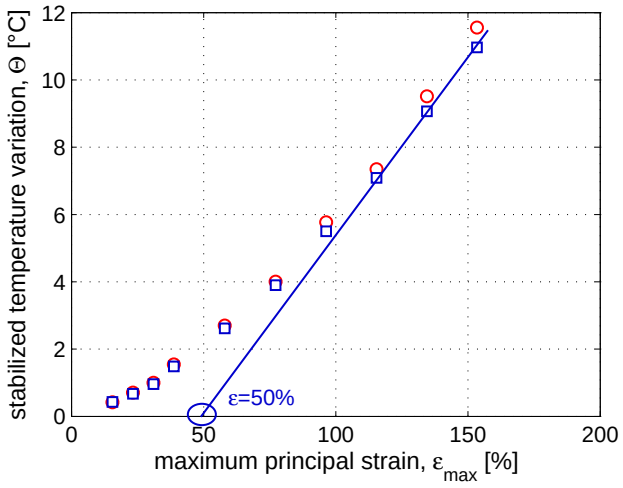

Figure 8: Empirical processing performed on material G.

metallic materials. This was expected as no clear fatigue limit is to be seen on the Wöhler curves obtained for elastomers. Moreover, rubbers exhibit many dissipative sources that will be discussed in paragraph 2.3, which makes the evaluation of the fatigue mechanism more difficult to point out than for metallics. Nevertheless, we were leading an exploratory study and we therefore adjusted an empirical analysis in order to meet the 10^6 cycles strain identified on a Wöhler curve (cf. figure 8 and column 4 of table 1). This protocol was then used to analyse the heat build-up curves obtained

reference	$\tan\delta$	$N_i(100\%)$	$\varepsilon_{10^6\,\text{cycles}}$	$\varepsilon_{evaluated}$	error
A	< 1	10^6	100%	100%	0%
B	2.3	237000	60%	69%	15%
C	3	170000	55%	62.5%	13.6%
D	4	123000	44%	55%	25%
E	6.6	83600	32%	30%	6.2%
F	12.9	52000	30%	30%	6.6%
G	12.9	16000	55%	50%	9%
H	23.3	8000	20%	30%	33.3%

Table 1: Comparison between the 10^6 cycles strain identified on a Wöhler curve $\varepsilon_{10^6\,\text{cycles}}$ and the estimated 10^6 cycles strain using the heat build-up test $\varepsilon_{evaluated}$.

from seven other materials, presented on figure 9. The results and the

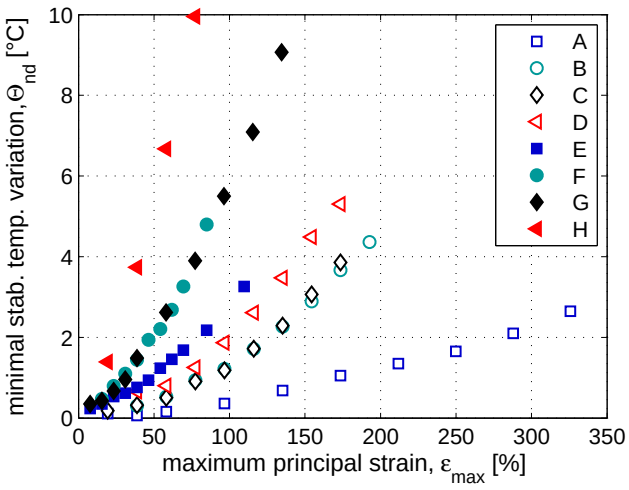

Figure 9: Heat build-up curves for materials A to H.

material data are afforded in table 1. It can be observed from the good agreement with the values provided by the Wöhler curves that the proposed graphical analysis is giving surprisingly good results. What can also be noticed is that the materials used present the same ranking from a fatigue point of view or from a viscous point of view (evaluated from their $\tan\delta$). As this fact was observed for the other tested materials (not presented here), a not yet resolved question is: what is really measured during a heat build-up test? To give some clues on that question, other tests have been performed on specifically selected materials showing either the same $\tan\delta$ but different fatigue resistances, or the same fatigue resistance but with different $\tan\delta$. This is what is presented in the next paragraph.

2.3. Sensitivity of the empirical protocol to the viscous dissipation

Rubber-like materials are known to be hysteretic materials at a macroscopic scale, which means that some energy is dissipated and/or stored during one loading cycle. This hysteresis is not well explained and can be justified by several explanations:

(a) Mullins effect [11]
(b) crystallization under strain [12]
(c) viscosity [13]
(d) plasticity [14]
(e) damage [15]

The contribution of each of these sources is not clearly defined yet but it is generally assumed that viscosity is one of the most important [13] and is a first order parameter. To check this assumption, we performed heat build-up experiments on specifically selected materials that have equivalent viscous dissipation potential (evaluated from the $\tan\delta$ value) and different fatigue lifetimes and materials that have different viscous dissipation potentials (evaluated from the $\tan\delta$ value) and equivalent fatigue lifetimes. The figure 10 shows the experimental curves obtained on materials having different $\tan\delta$ but the same fatigue lifetime. It seems that the empirical protocol is working quite well. Considering now materials that have the same $\tan\delta$

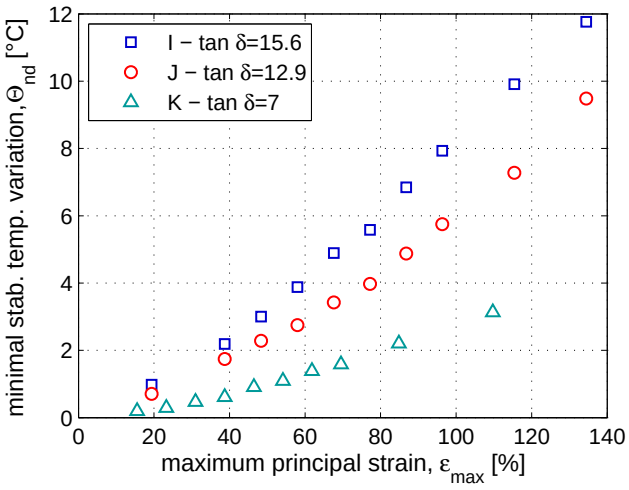

Figure 10: Heat build-up curves for materials having the same fatigue lifetime but different $\tan\delta$.

but different fatigue lifetimes (see figure 11), the curves obtained are very similar and can not lead to isolate the fatigue lifetime. It can therefore be concluded that even if the rough estimation analysis presented above has proven to be quite effective for several materials, a clear separation between viscous dissipation and a dissipation related to the fatigue resistance is far less easy to identify for rubber-like materials than for metallic materials. Moreover, this protocol is giving only one point of the Wöhler curve, which is clearly not enough as the slopes of these curves may be quite different depending on the nature of the tested rubber [16]. Nevertheless, the heat build-up measurements are useful to identify the parameters of constitutive models including some dissipation sources (viscosity, plasticity, damage) because these tests provide both mechanical and thermal data. Moreover, a

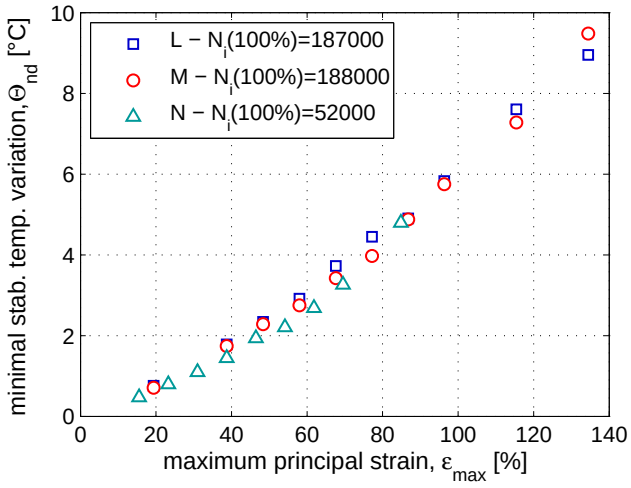

Figure 11: Heat build-up curves for materials having the same $\tan\delta$ but different fatigue lifetime.

stabilization of the temperature increase was always observed (at the limited frequency imposed) and this stabilization means that the dissipation source is nearly constant: an equilibrium between what is lost by conduction and convection and induced by cyclic loadings is reached. It is also clear that the global dissipated energy could not be directly related to the fatigue damage and that the description of the damage at lower scales is mandatory. In paragraph 3 we present how the temperature measurements can be useful if some more information on the fatigue damage evolution at a microscopic scale is provided.

3. Evolution of fatigue damage using X-ray microtomography

3.1. Principle of the critical energy criterion and scope of the investigation

Basically, fatigue design of rubber components requires two steps: first choose a mechanical parameter: strain [7, 10], stress [17–19], strain energy [18, 20], ..., and second perform several fatigue tests on samples of different geometries, under different sollicitations, in order to generate Wöhler curves, plotting the value of the chosen parameter with respect to the number of cycles needed to break the sample or to initiate a crack. A power law is then usually identified, relating the parameter to the number of cycles and is to be applied to design industrial components. It is important to note that the fatigue parameter can be different from the initiation criterion. This

initiation criterion is usually a damage parameter, chosen for its ability to be summed in order to analyze variable fatigue solicitations. Depending on the materials, this parameter could be the dissipated energy [21–23], the cumulated plastic strain [24] or a scalar damage parameter associated with an evolution law [25]. Here, we will keep the maximal strain chosen formerly as the fatigue parameter and we will use an initiation criterion based on the cumulated dissipated energy. The principle of the approach is therefore very classic and simple: whatever the fatigue parameter may be, the cumulated dissipative energy needed to initiate a crack will be a constant, called here CDE (Critical Dissipated Energy). This energy based approach is close to the one proposed by [26] based on a Cracking Energy Density (CED) which is cumulated along the cycles and aims at being representative of the crack opening. It can also be related to the approach proposed by [15].

In elastomers, the energy dissipated evolves during the fatigue tests but reaches a stabilized value after the number of cycles needed to stabilize the rise of temperature induced by the heat build-up. Once this stabilization step is achieved, the dissipated energy measured along the fatigue test is almost a constant, for a given global displacement. This is confirmed by the stabilization of the heat build-up along a fatigue test, showing that the dissipation sources are constant (see figure 5(a)). It is therefore possible to write that:

$$\text{CDE} = N_i \cdot E_{fatigue,diss/cycle} \tag{1}$$

with CDE the Critical Dissipated Energy considered as an intrinsic constant, N_i the number of fatigue cycles needed to reach the initiation (according to a given experimental criterion) and $E_{fatigue,diss/cycle}$ the energy dissipated per cycle by the fatigue mechanisms, which is a function of the maximum strain.

As illustrated in paragraph 2, the dissipated energy is not easy to relate to the fatigue durability of elastomers as it does not depend only on the fatigue mechanisms. Several materials exhibiting the same dissipated energy per cycle will not necessarily have the same fatigue lifetime. It is consequently difficult to propose an experimental evaluation of the value of $E_{fatigue,diss/cycle}$ introduced in equation 1 since both a global evaluation of the dissipated energy and reliable micro-structural data on the fatigue mechanisms are required. The proposed approach is therefore:

- to use micro-structural measurements of the fatigue defect population, as it is well stated in the literature that the fatigue mechanisms for

both initiation and propagation at a micro-scale are strongly related to the defect population [16, 27–32];

- to use the heat build-up measurements as an evaluation of the dissipated energy during cyclic and fatigue tests.

We focus here on a polychloroprene rubber, which was studied during the heat build-up campaign and which fatigue damage evolution was followed by X-ray computed tomography [1]. The samples used for the fatigue tests, the heat build-up tests and the X-ray tomography measurements were obtained from the same batch of material. The complex shape of the specimen (see figure 1) ensured that the initiation zone is well controlled and is located in the thinner section. Temperature measurements were also achieved in that zone, and the defect populations presented in the following are only the ones observed in slices of 1 mm thick, located the middles of the samples (see figure 12). It is therefore possible to link the observations made for the

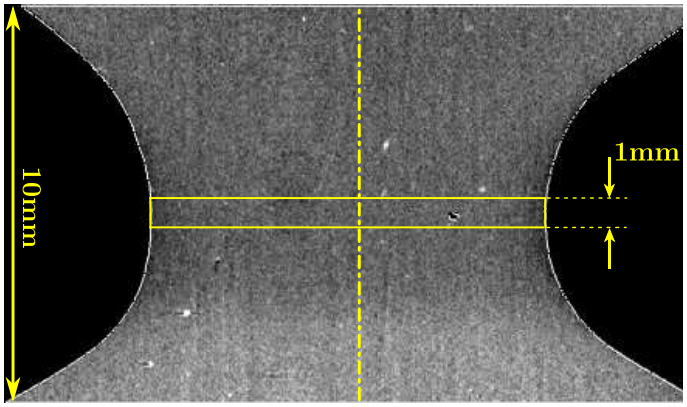

Figure 12: Studied zone for the temperature and tomography measurements.

fatigue initiation lifetime, the temperature rise and the defect population. In the following, the defect population dependency on the maximum strain and on the number of cycles is detailed (paragraph 3.2), then the main assumptions made to evaluate $E_{fatigue,diss/cycle}$ (paragraph 3.3)is presented and finally, the identification of the Critical Dissipated Energy is achieved in paragraph 3.4. Finally a validation of our method is proposed by comparing the initiation curve built from our approach to the experimental fatigue results.

3.2. Defect volumic density

X-ray computed micro-tomography was used to investigate the fatigue damage occurring in a polychloroprene rubber [1]. This non destructive technique allowed us to study the evolution of the defect population along the fatigue cycles and its dependency on the maximum local strain. This study revealed that the defect volumic density depends both on the number of cycles and on the maximum local strain. It also showed that the defect density was evolving quickly during the first step of the fatigue test (less than 10%) and was then evolving very slowly. The value obtained after a few thousands cycle is therefore representative of the initiation value. Moreover, the evolution of the defect volumic density with respect to the maximum strain was measured. This curve is plotted on figure 13 and was obtained from several samples and for several fatigue test durations. We

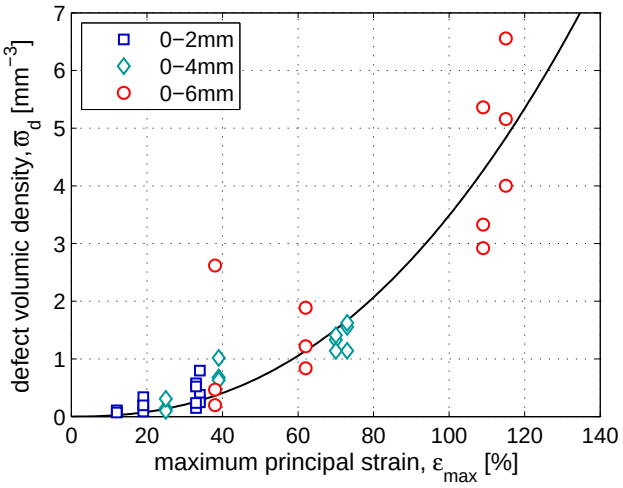

Figure 13: Evolution of the defect population density with respect to the maximum principal strain. The legend values correspond to the macroscopic displacement applied to the specimen.

also checked that the average radius of the defects was not evolving much along the fatigue test and was not dependent on the maximum strain. The defect volumic density is used here to be more precise but as the studied volume is the same for all the samples, it can also be seen as the number of defects. We therefore know the dependency of the defect density on the maximum strain but we still do not know how the material dissipates energy.

3.3. Evaluation of the energy dissipated by a defect population

Once the defect population and its evolution with respect to the maximum local strain are described, a first way to evaluate $E_{fatigue,diss/cycle}$ would be to write that :

$$E_{fatigue,diss/cycle} = \sum_{defects} E^d_{diss/cycle} \tag{2}$$

with $E^d_{diss/cycle}$ being the dissipated energy by each defect. The next step combines Finite Element simulations [28, 33] and homogeneization techniques [34]. This is maybe the closest approach from the microscopic mechanisms but it is still meeting very big difficulties. The first problem comes from the assumed equivalence between a given population of defects exhibiting different sizes and shapes and a homogeneous population of an equivalent defect. Then, the evaluation of the energy dissipated by a given defect meets the complexity of elastomeric materials (shape of inclusions, matrix visco-hyper-elasticity, low compressible behaviour, difficulty to identify the interphase behaviour, necessity to take the inclusion interactions into account, ...). At last, the dissipative sources related to a defect in an elastomeric matrix are still not well identified (growth of the cavity, matrix inelasticity, friction at the interface ...) and are therefore difficult to evaluate. Here, we have chosen a much more phenomenological approach: we chose to relate the total dissipated energy (evaluated from the stabilized rise of temperature) to the energy dissipated by the defect population.

The first hypothesis assumes that the ratio between the total dissipated energy and the one related to the fatigue mechanisms (whatever the kind of dissipation it leads to) is linearly dependant on the defect density. It would then come:

$$E_{fatigue,diss/cycle} = A \cdot \varpi_d \cdot V \cdot E_{diss/cycle} \tag{3}$$

With A being a constant, ϖ_d the defect volumic density in the central zone of the sample, V the considered volume and $E_{diss/cycle}$ the total dissipated energy during one fatigue cycle in that volume. The second hypothesis is that the total dissipated energy is evaluated from the temperature rise only. This strong assumption is supported by the very low thermal conductivity of the material and because we consider here only the rise of temperature linked to the dissipation, with no thermoelastic couplings (see paragraph 1.3.1). This point will of course be further investigated but this assumption is taken as a first rough evaluation. We could consequently write that:

$$E_{diss/cycle} = B \cdot \Theta_{nd} \tag{4}$$

With B a constant parameter and Θ_{nd} the stabilized minimum rise of temperature in the central zone of the sample, which is dependant on the maximum imposed deformation. This global evaluation is also required because:

- the rise of temperature, measured at the skin, is an average value of the dissipation sources that are located in the volume underneath;
- the defect volumic density is also defined as an average value for a given volume.

From equations 1, 3 and 4, it would then come:

$$\mathrm{CDE} = N_i \cdot A \cdot \varpi_d \cdot V \cdot B \cdot \Theta_{nd} \tag{5}$$

Which can also be written as:

$$N_i \cdot \varpi_d \cdot \Theta_{nd} = c^{ste} \tag{6}$$

for a given volume.

3.4. Experimental validation of our approach

In the following we will use the figure 13, 14 and 15 in order to evaluate the numerical values of the terms in equation 6. The initiation lifetime is taken from the Wöhler curve, the defect volumic density is obtained from the curve fitted on the X-ray tomography measurements and the rise of temperature is obtained from the heat-build up curve. The first step is to identify the value of the constant of equation 6, that is given in table 2. In

ε_{max}	N_i	ϖ_d	Θ_{nd}	$N_i \cdot \varpi_d \cdot \theta_{nd}$
30%	10^6 cycles	$0.2\,\mathrm{mm}^{-3}$	2.2°C	440000
70%	$3.5{\cdot}10^4$ cycles	$1.5\,\mathrm{mm}^{-3}$	8.2°C	430500
110%	$6.5{\cdot}10^3$ cycles	$4.5\,\mathrm{mm}^{-3}$	15.2°C	444600

Table 2: Evaluation of the constant (equation 6)

order to validate the approach, we then evaluate the product of equation 6 for several maximum local strains. It can be observed from table 2 that the values obtained are very similar. The second step of validation was to build an initiation curve from equation 6, using one of the constant evaluated (for example 440000, obtained for a 2 mm displacement) and power laws fitted on

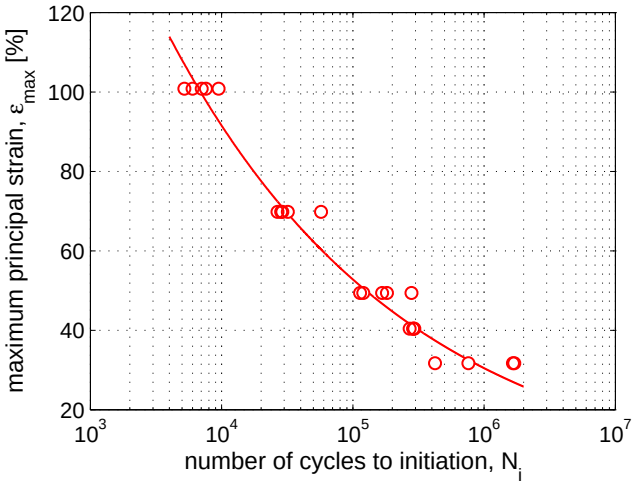

Figure 14: Wöhler curve of the studied polychloroprene rubber.

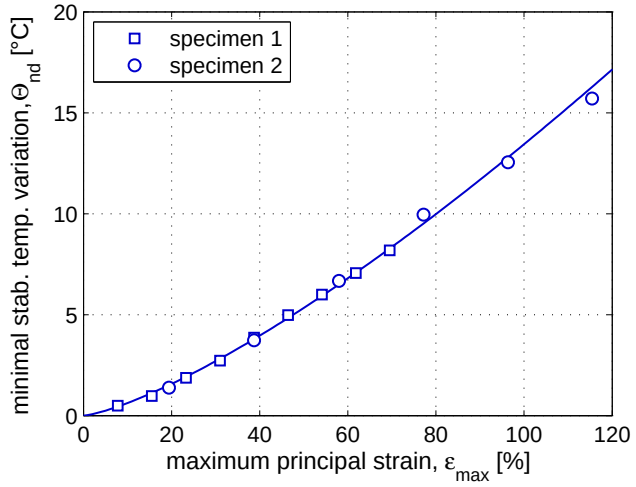

Figure 15: Heat build-up curve of the studied polychloroprene rubber.

the curves of figure 13 (defect volumic density) and 15 (stabilized minimum temperature rise). The curve obtained is plotted on figure 16 and exhibits a very good correlation with the other experimental points. As the value obtained from equation 6 was varying a little from a condition to another, we also plot the same curve, obtained with a variation of 15% from the value of the constant used to build the curve. It illustrates that the variations observed in table 2 lead to very few differences of the reconstructed initiation

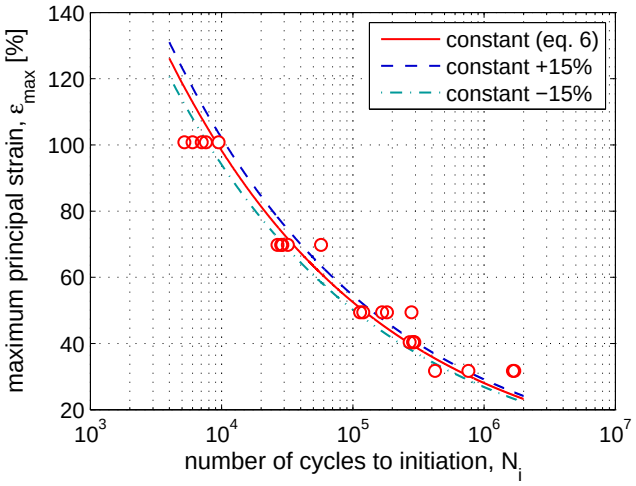

Figure 16: Prediction of the Wöhler curve using the proposed approach.

lifetime curve.

Despite the very strong hypotheses used here and that need to be further investigated, this approach leads to convincing results and seems therefore very promising because it could shorten very much the determination of the fatigue properties of an elastomeric material. With about 6 samples in order to propose a reliable fit of the evolution of the defect population along the maximum strain (5 submitted to an interrupted heat build-up protocol and then analysed by X-ray tomography, 1 that is pushed until the initiation in order to have a value for the energy constant) and within 3 days (one day for mechanical testing and 2 for X-ray measurements and analysis) it could be possible to evaluate the full initiation lifetime curve. The dispersion observed for fatigue tests might also be deduced from the dispersion on the defect density, as the rise of temperature is very repeatable. Nevertheless, the proposed approach is of course to be validated on several materials, which is currently undertaken.

Conclusions

In this study we focused on the development of a heat build-up test, which relates the maximum principal strain to the temperature rise. A very first step was to propose an accurate measurement protocol suitable for large displacements and that could discriminate the temperature rise induced by cumulative dissipation from the thermo-elastic contribution. More than fif-

teen industrial materials were tested in order to experiment the ability of that kind of test to be representative of the fatigue resistance of elastomers. These tests provided promising results but a quick analysis is still made delicate by the highly viscous nature of these materials . In order to propose a physically based evaluation of the dissipated energy related to the fatigue defects, we used here the results from another paper [1]. The defect volumic density was used to evaluate the ratio of the total dissipated energy, deduced from the heat build-up measurements, that could be related to the damage. An energy based fatigue criterion is then proposed and validated for a polychloroprene rubber. The correlation between the fatigue results obtained from a classical Wöhler curve and those from the proposed approach is excellent and clearly calls further developments and validations on other materials. This study also illustrated that the heat build-up test seems to be an appropriate tool to identify the parameters of constitutive models including dissipation, as both mechanical and thermal responses are analysed. It also proved how valuable micro-tomography measurements can be in order to understand what happens during the heat build-up tests and to feed the mechanical models with damage kinetics.

Acknowledgements

The authors would like to thank the Brittany region for its financial support and all the actors of the FEMEM project. A special thank to P. Laguillaumie for his careful reading.

References

[1] V. Le Saux, Y. Marco, S. Calloch, P. Charrier, Evaluation of the fatigue defect population in an elastomer using X-ray computed micro-tomography, Journal of Polymer Engineering and Science Submitted (October 2009).

[2] C. Doudard, S. Calloch, P. Cugy, A. Galtier, F. Hild, A probabilistic two-scale model for high-cycle fatigue life predictions, Fatigue & Fracture of Engineering Materials & Structures 28 (2005) 279–288.

[3] M. Luong, Infrared thermography of fatigue in metals, SPIE 1682 (1992) 222–233.

[4] J. Joule, On some thermodynamics properties of solids, Philosophical Transactions of the Royal Society of London 149 (1859) 91–131.

[5] R. Anthony, R. Caston, E. Guth, Equations of state for natural and synthetic rubber-like materials. I. Unaccelerated natural soft rubber, The Journal of Physical Chemistry 46 (1942) 826–840.

[6] L. Treloar, The physics of rubber elasticity (third edition), Oxford (UK) : Oxford University Press, 1975.

[7] S. Cadwell, R. Merrill, C. Sloman, F. Yost, Dynamic fatigue life of rubber, Industrial and Engineering Chemistry 12 (1940) 19–23.
[8] B. Roberts, J. Benzies, The relationship between uniaxial and equibiaxial fatigue in gum and carbon black filled vulcanizates, Proceedings of Rubbercon'77 (1977) 2.1–2.13.
[9] E. Ostoja Kuczynski, Comportement en fatigue des élastomères : application aux structures antivibratoires pour l'automobile, Ph.D. thesis, Ecole Centrale de Nantes, Université de Nantes, 2005.
[10] E. Ostoja Kuczynski, P. Charrier, E. Verron, L. Gornet, G. Marckmann, Crack initiation in filled natural rubber: experimental database and macroscopic observations, in: Constitutive Model for Rubber III, London (UK), 3–10, 2003.
[11] J. Diani, B. Fayolle, P. Gilormini, A review on the Mullins effect, European Polymer Journal 45 (2009) 601–612.
[12] J. Marchal, Cristallisation des caoutchoucs chargés et non chargés sous contraintes : effet sur les chaînes amorphes, Ph.D. thesis, Université de Paris XI Orsay, 2006.
[13] J. Bergström, M. Boyce, Constitutive modeling of the large strain time-dependend behavior of elastomers, Journal of the Mechanics and Physics of Solids 46 (1998) 931–954.
[14] C. Miehe, J. Keck, Superimposed finite elastic-viscoelastic-plastoelastic stress response with damage in filled rubbery polymers. Experiments, modelling and algorithmic implementation, Journal of the Mechanics and Physics of Solids 48 (2000) 323.365.
[15] J. Grandcoin, Contribution à la modélisation du comportement dissipatif des élastomères chargés : d'une modélisation micro-physiquement motivée vers la caractérisation de la fatigue, Ph.D. thesis, Université d'Aix-Marseille II, 2008.
[16] W. Mars, A. Fatemi, A literature survey on fatigue analysis approaches for rubbers, International Journal of Fatigue 24 (2002) 949–961.
[17] C. Lu, Etude du comportement mécanique et des mécanismes d'endommagement des élastomères en fatigue et en fissuration par fatigue, Ph.D. thesis, CNAM, 1991.
[18] F. Abraham, T. Alshuth, S. Jerrams, The effect of minimum stress and stress amplitude on the fatigue life of non strain crystallising elastomers, Materials & Design 26 (2005) 239–245.
[19] N. Saintier, G. Cailletaud, R. Piques, Multiaxial fatigue life prediction for a natural rubber, International Journal of Fatigue 28 (2006) 530–539.
[20] F. Lacroix, S. Méo, G. Berton, F. Chalon, A. Tougui, N. Ranganathan, A local criterion for fatigue crack initiation on chloroprene rubber : approach in dissipation, in: ECCMR IV, Stockholm (Sweden), 77–82, 2005.
[21] F. Ellyin, K. Golos, Multiaxial fatigue damage criterion, Journal of Engineering Materials and Technology 110 (1988) 63–68.
[22] G. Fargione, A. Geraci, G. La Rosa, A. Risitano, Rapid determination of the fatigue curve by the thermographic method, International Journal of Fatigue 24 (2002) 11–19.
[23] E. Charkaluk, A. Bigonnet, A. Constantinescu, K. Dang Van, Fatigue design of structures under thermomechanical loadings, Fatigue & Fracture of Engineering Materials and Structures 25 (12) (2002) 1199–1206.
[24] I. Papadopoulos, Fatigue polycyclique des métaux: une nouvelle approche, Ph.D.

thesis, Ecole Nationale des Ponts et Chaussées, 1987.
[25] J. Lemaitre, J. Chaboche, Aspect phénoménologique de la rupture par endommagement, Journal de Mécanique Appliquée 2 (3) (1978) 317–365.
[26] W. Mars, Multiaxial fatigue of rubber, Ph.D. thesis, University of Toledo, 2001.
[27] J. Busfield, A. Thomas, M. Ngah, Application of fracture mechanics for the fatigue life prediction of carbon black filled elastomers, in: Constitutive Model for Rubber, Rotterdam (The Netherlands), 249–256, 1999.
[28] N. Saintier, Fatigue multiaxiale dans un élastomère de type NR chargé : mécanismes d'endommagement et critère local d'amorçage de fissure, Ph.D. thesis, Ecole Nationale Supérieure des Mines de Paris, 2001.
[29] J. Le Cam, B. Huneau, E. Verron, L. Gornet, Mechanism of fatigue crack growth in carbon black filled rubber, Macromolecules 37 (2004) 5011–5017.
[30] J. Le Cam, E. Verron, B. Huneau, L. Gornet, Micro-mechanism of fatigue crack growth: comparison between carbon black filled NR SBR, in: Constitutive model for rubber IV, Stockholm (Sweden), 115–120, 2005.
[31] N. Saintier, G. Cailletaud, R. Piques, Crack initiation and propagation under multiaxial fatigue in a natural rubber, International Journal of Fatigue 28 (2006) 61–72.
[32] K. Le Gorgu Jago, Fatigue life of rubber components: 3D damage evolution from X-ray computed microtomography, in: Constitutive Model for Rubber V, Paris (France), 173–177, 2007.
[33] Y. Fukahori, W. Seki, Stress analysis of elastomeric materials at large extensions using the finite elements methods. II: Stress and strain distribution around rigid spherical particles, Journal of Materials Science 28 (1993) 4471–4482.
[34] B. Omnès, S. Thuillier, P. Pilvin, G. Gillet, Non-linear mechanical behavior of carbon black reinfored elastomers: experiments and multiscale modelling, Plastics, Rubber and Composites 37 (2008) 251–258.

A. Compound specifications

Reference	Polymer	Fillers	Vulc. System	Parts
A	NR	0	Conv.	research only
B	NR	CB (22 phr)	Conv.	PTMS
C	NR	CB (21 phr)	S-EV	PTMS
D	NR	CB (28 phr)	EV	PTMS
E	NR	CB (39 phr)	EV	PTMS
F	NR	CB (55 phr) Si (12 phr)	EV-S-EV	PTMS
G	NR	CB (43 phr)	Conv.	PTMS
H	CR	CB (3 phr) Si (23 phr)	Conv.	Offshore
I	NR	CB (56 phr)	S-EV-Conv.	PSS
J	NR	CB (50 phr)	S-EV-Conv.	PSS
K	NR	CB (25 phr)	S-EV-Conv.	PSS
L	NR	CB (55 phr)	S-EV-Conv.	PSS
M	NR	CB (50 phr)	S-EV-Conv.	PSS
N	NR	CB (55 phr) Si (12 phr)	EV-S-EV	PTMS

Table 3: Compound specifications. NR (Natural Rubber), CR (Polychloroprene Rubber), CB (Carbon Black), Si (Silica), Conv. (Conventional), S-EV (Semi-efficient), EV (Efficient), PTMS (Power Train Mouting System), PSS (Power Strut System).

ANNEXE

F

Article sur la description des populations de défauts

Dans cette annexe, nous présentons un article publié par Le Saux et al. (2010a) dans le journal Polymer Engineering & Science*. Celui-ci traite de la description des populations sous sollicitations cycliques que nous avons évoquées dans le paragraphe 3.3 du chapitre 3. L'article a été accepté en Août 2010 et est donné sous la forme d'un* preprint.

Evaluation of the fatigue defect population in an elastomer using X-ray computed micro-tomography

V. Le Saux[a], Y. Marco[*,a], S. Calloch[a], P. Charrier[b]

[a] *Laboratoire Brestois de Mécanique et des Systèmes (EA 4325), ENSIETA/Université de Brest/ENIB, 2 rue F. Verny 29806 Brest Cedex 9, France*
[b] *Trelleborg Modyn, Z.I. Nantes Carquefou BP 419, 44474 Carquefou Cedex, France*

Abstract

As elastomeric materials are heterogeneous by nature, their fatigue behavior is strongly driven by the initiation and the growth of cavities. In this study X-ray micro-tomography is used to describe the fatigue mechanisms at a micro-scale. This non destructive method has already been widely applied to elastomeric materials to control the fillers size and dispersion or to analyze the cavitation induced under high hydrostatic pressure fatigue loading, for example. Here, this technique is used with a good resolution to analyse the evolution of the defects population during a fatigue campaign on hourglass shaped axisymetric specimens. The initiation and propagation mechanisms are clearly shown on 3D observations, and the influences of the maximum principal strain and of the number of cycles on several parameters (size repartition, porosity, defect volumic density) are investigated. A scenario for the fatigue damage evolution is proposed and some fatigue initiation criteria are finally discussed, using the results obtained at the microscopic scale.

Key words: fatigue analysis, microstructure, X-ray, elastomers

Introduction

Rubber-like materials are extensively used in many industrial fields, imposing their ability to undergo large deformations, their resistance to aggressive environments, and their damping behaviour often coupled with a

[*]Corresponding author. Tel.: 33 (0)2 98 34 89 11; Fax: 33 (0)2 98 34 87 30
Email address: Yann.Marco@ensieta.fr (Y. Marco)

good fatigue resistance. This latter property is still not well understood for several reasons: the deformations encountered are extremely large, the material is obtained from a recipe mixing several components, its properties depend on the curing and injection parameters and the phenomena involved couple mechanical, thermal and chemical effects, etc. [1, 2]. In this paper, the influence of the mechanical parameters on the fatigue resistance is investigated, with as less as possible coupled effects like ageing or crystallization. Coming from the heterogeneous nature of elastomeric materials (fillers, oxides, additives helping the processing, natural inclusions, etc.) the fatigue properties are strongly dependant on the existing flaws, that can be considered as the main damage initiation locations [3, 4]. The roles of these flaws are usually studied by SEM analysis [5–7], which provides interesting data but can hardly be representative of the global damage [8]. In this study, we will use X-ray micro-tomography (X-ray CT). X-ray CT is a method used for a long time in the medical field and which has been increasingly utilized in recent years in the field of materials science. This non-destructive observation technique enables to study 3D imaging of material microstructures [9–11] as well as pores distribution [12, 13]. The technique has also proven to be a useful tool in assessing the micromechanisms of fatigue crack growth [14] and damage evolution [15]. Dealing with elastomeric materials, a few studies already exists either focused on the observation of inclusions dispersion or on the study of the damage evolution. Remarkable works were done on the latter point during the last years, proving how useful this technique could be to study cavitations at a mesoscopic scale for high hydrostatic fatigue conditions [2] or to detect local changes of physical and chemical properties by measuring X-ray attenuation [16–20]. Unfortunately, the quite low resolution (about 200 μm) of the medical scanner usually used prevented the detection of small defects (about 40 μm) that are associated to the fatigue initiation [3, 21–23]. One of the most interesting article on the use of X-ray CT to follow the damage evolution has been published recently [8] and provides very useful information on the fatigue mechanisms with a higher resolution (detection of defects with a diameter of about 15 μm).Nevertheless, quantitative data describing the dependency of the defect population on the fatigue parameters are still missing, which limit the proposal and validation of models trying to describe the initiation and the growth of fatigue cavities. The purpose of this paper is therefore to use computed X-ray micro-tomography with a high enough resolution (detection of defects with a radius of about 13 μm) to describe in a 3D manner

the fatigue mechanisms and to propose a description of the evolution of the defect population in a polychloroprene rubber submitted to fatigue loading. This technique is used here to analyse hourglass shaped samples previously submitted to several fatigue loading conditions. The initiation and propagation mechanisms are investigated. Then, the influences of the maximum local strain and of the number of cycles on representative parameters (cavities distribution, average volume, porosity, volumic number of defects) are studied and a scenario is proposed for the damage evolution. Based on these results, an evaluation of some basic fatigue criteria is proposed.

1. Materials and testing

1.1. Materials and specimen

The material used here is a polychloroprene rubber (CR) formulated with silica and a low percentage of carbon black. The main idea was to use a material with a not too high fatigue durability in order to reduce the tests duration and with a low carbon black ratio in order to make the X-ray tomography analysis easier (the density of the carbon blacks is nearly the same as the elastomeric matrix). Table 1 gives a few elements on the considered material. Hourglass shaped specimens were manufactured from

density ($g{\cdot}cm^{-3}$)	shore (A) hardness	UTS (MPa)	Strain at break (%)
1.4	68	17.4	670

Table 1: Room temperature properties

a single batch in order to ensure the reliability of mixing and moulding conditions. The geometry of the specimen is given on figure 1. This kind of specimen (called AE2 in the following) was chosen for three main reasons: it is classically used to obtain Wöhler curves; the initiation and break zone is well mastered and is located in the thinner section; its complex geometry leads to different strain and stress states along its axis, even under uniaxial tensile tests, and will make the X-ray CT analysis richer.

1.2. Micro-tomography measurements and analysis

The goal here was clearly not to achieve nano-tomography measurements, as may be found elsewhere [24], using a synchrotron beam, but to study the fatigue phenomena in larger samples. The device used here is powerful but more industrial for two reasons: synchrotron devices are not

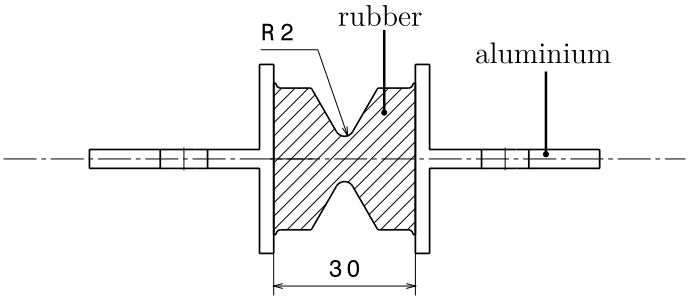

Figure 1: AE2 specimen

very accessible (limited beam time) and the analyzed volumes are very limited, which involves to cut the specimens. Thus, we used a X-ray CT device whose resolution is high enough compared to the defect sizes classically measured by SEM measurements (range from 10 to 400 μm). The experimental settings of the Phoenix device used (v|tome|x L 240) are given in table 2. The samples were placed at a distance of 828 mm from a Perkin-Elmer CCD

X-ray tube voltage	180 kV
current	116 μA
scan time	$\approx$ 30 min
rotation	360° by step of 0.45°
resolution	1 px = 21μm

Table 2: X-Ray micro-tomography experimental settings

detector with a 1024 $\times$ 1024 pixel array. Eight thousands radiographs were taken at regular increments over a 360° rotation, the exposure time was 400 ms/image and for each radiography, the first image was excluded in order to avoid the detector remanence, and 4 images were then averaged. The spatial resolution of the technique, *i.e.* the volume of the smallest element (isotropic voxel) in the reconstructed 3D images was $9.2{\cdot}10^{-6}$mm^3. The volume of material investigated for each sample was around 2700 mm^3. A dedicated commercial software (myVGL 2.0) performing 3D image analysis was then used to study the inclusions and the defects population of the samples. The grey level images obtained after reconstruction were thresholded in order to separate the pores from the rest of the material. The resulting binary images were automatically analysed and the concentration in the studied volume as well as individual parameters such as volume, surface, aspect ratios, axis of inertia were computed. A special care was taken

to reduce measurement artifacts. The minimal size detected for defects was adjusted to 4 voxels (*i.e.* an equivalent radius of 13 μm) to ensure an effective detection. All the specimens were slightly stretched (relative displacement of 2 mm of the inserts) in order to open the cavities and to make them easier to detect. This stretching was carefully achieved just before the measurement in order to prevent the opening of the cavities under static conditions during the time left between the mechanical test and the X-ray CT observation.

It is important to notice that, in this study, no samples were submitted again to fatigue loading after the X-ray CT measurements. This choice implies that no specific defects can be followed as the number of cycles increases, but makes sure that the exposition to X-ray is not influencing the material behaviour (chains scission and crosslinking) and to therefore take into account the intrinsic dispersion.

1.3. Fatigue campaign

Fatigue tests were achieved at room temperature, on an INSTRON 1342 hydraulic machine, equipped with hydraulic grips. The frequency of the tests was 2 Hz in order to limit the heat build-up effect and the experiments were displacement controlled. The temperature of the specimens were measured by an infrared camera and the maximum rise of temperature encountered was 15°C. This value, coupled with a low number of cycles should limit any coupled thermal or chemical effect during the test. The load ratio was fixed to R=0 in order to limit the low crystallization effect that may be encountered for polychloroprene rubber [2].

First, several fatigue tests were conducted to build a Wöhler curve with AE2 specimens, with the formerly detailed settings. Five specimens were tested at five strain levels. During the tests, the stiffness and the specimen temperature were recorded and a classical criterion on the stiffness loss rate [25] was used to detect the initiation. The Wöhler curve obtained is given on figure 2. Then, 3 macroscopic maximum displacements (X = 2, 4 and 6 mm) were chosen, associated with the respective numbers of cycles that lead to initiation (referenced Ni in the following). For each of these displacements, at least 5 interrupted tests were achieved (some of them were made twice). The tests were stopped after 5 cycles and after 10, 25, 50, 100% of Ni (obtained from the Wöhler curve). Figure 3 illustrates this fatigue campaign.

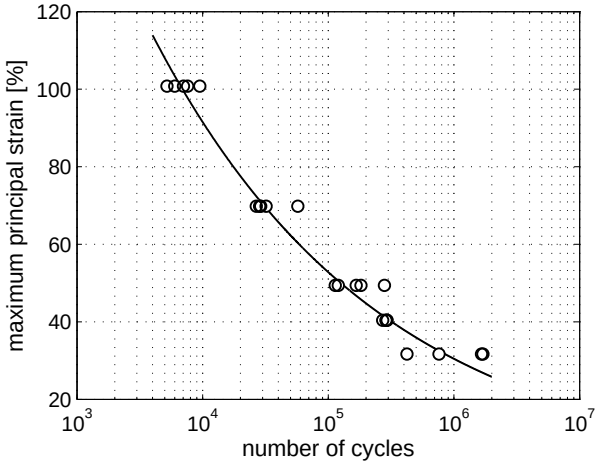

Figure 2: Wöhler curve of the studied materials.

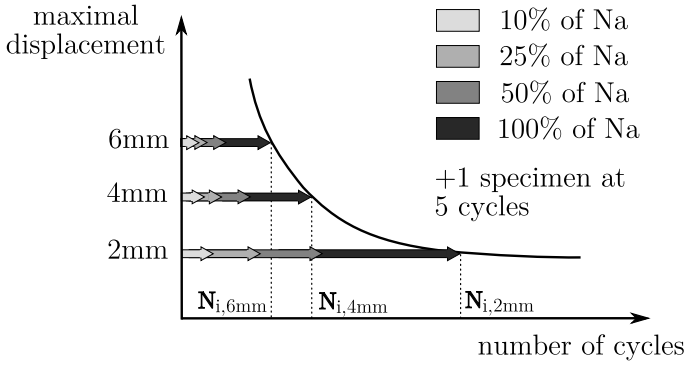

Figure 3: Interrupted fatigue tests.

2. Results

2.1. Illustration of initiation and propagation mechanisms for fatigue loading

2.1.1. Initiation mechanisms

Figure 4 shows a typical result obtained by X-ray CT on a sample with no clear cracks but exhibiting a large number of cavities. In this paragraph, the defects created for samples at early stages of degradation (5 cycles or 10% of Ni) are specifically studied in order to evaluate the initiation mechanisms. Cavities were found to initiate from flaws of the material, either inclusions or agglomerates, which is a classical result for fatigue. The most often encountered inclusions and agglomerates in the studied material

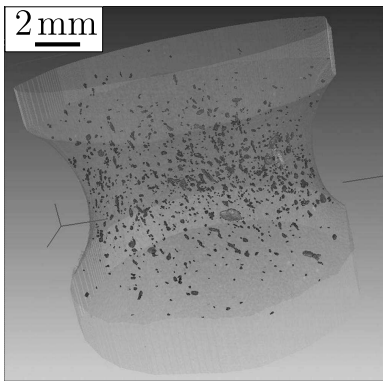

Figure 4: Example of cavities mapping obtained with computed X-ray micro-tomography.

are composed of ZnO (white spots, density = 5.6 g/cm^3), SiO_2 (gray agglomerates, density = 2.2 g/cm^3) and carbon black based ones (dark spots, density = 1.9 g/cm^3). The observations lead to identify the main damage processes.

The most often encountered mechanism is related to voids creation between two or more close flaws oriented along the tensile direction. These voids occurred whatever the nature of the involved particles (ZnO, SiO2 and carbon black), as illustrated on figure 5. In a few cases, one can ask if the

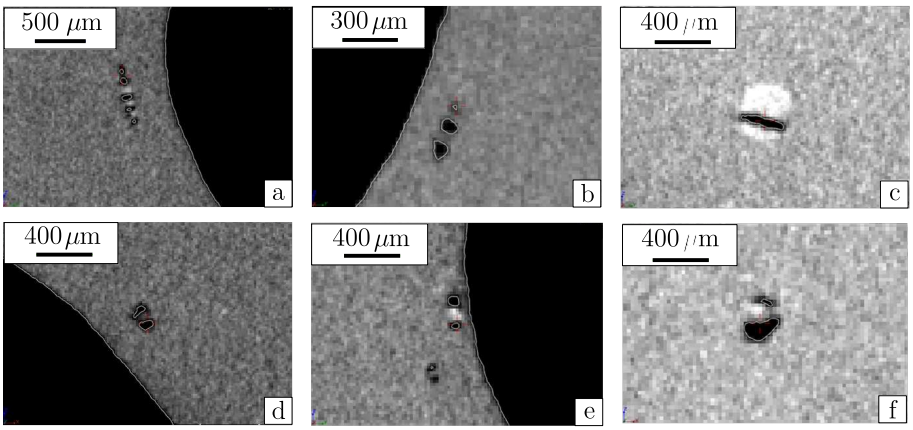

Figure 5: Creation of voids between close flaws (a, b, c) or in the polar zones of inclusion (d, e, f).

voids are created, not from the cavitation mechanism but from the break of the agglomerates. Voids also very clearly appear in the polar zones of inclu-

sions (Fig. 5), especially in the case of isolated inclusions. Some voids are also observed without any clear agglomerates or inclusions in their neighbourhood. This could either be explained by flaws with a radius smaller than 13 μm that are not detected due to the resolution of the Phoenix device or from carbon black agglomerates that are always difficult to point out clearly because they have nearly the same density as the matrix. Some authors also propose that these voids could be generated by over-cured zones of the elastomeric matrix [26] resulting in a local higher modulus and a local inclusion-like behaviour. The global overview accessible by X-ray CT exhibits that no preferential zones (for example a ring near the surface sample or specific location due to the location of the injection pin point) are to be seen and that no clear influence of the process can be involved (except for the presence of agglomerates that can hardly be avoided by any type of mixing process). This last point will be further investigated as the injection point location, the flow history and the mould parting zone are likely to influence the inclusions spatial repartition.

The present observations meet the conclusions obtained from SEM measurements [4, 26]. Depending on the strength of the link between the inclusion and the matrix [27], the voids will be created at the interface (decohesion) or in the matrix (cavitation). It also shows that the probability to observe cavitation between close particles, well aligned with the solicitation axis, is higher than around large size inclusions. This is confirming a recent study achieved on carbon black filled NR [8] using the same technique. This observation underlines that fatigue damage modelling by the mean of finite elements has to consider several inclusions to be representative [28] (not talking about shape or gradient effects). It is interesting to note that the sizes of these big defects, early created, are well correlated to the size of the initiation defects evaluated using inverse approaches based on fracture mechanics [21–23].

2.1.2. Propagation mechanisms

In paragraph 2.2, a specific study of the defects population, dealing with its evolution along the number of cycles, will be presented. The birth and growth of cavities will therefore not be detailed here but rather the already created cracks that were observed in several samples, either stopped right after the initiation or a little bit later. As underlined in paragraph 1.2, a single crack is not followed for several fatigue cycles as the X-ray CT measurements were always achieved on different samples. Figure 6 is consequently showing several radial spatial slices of the same cracks and not

the evolution of some cracks along time.

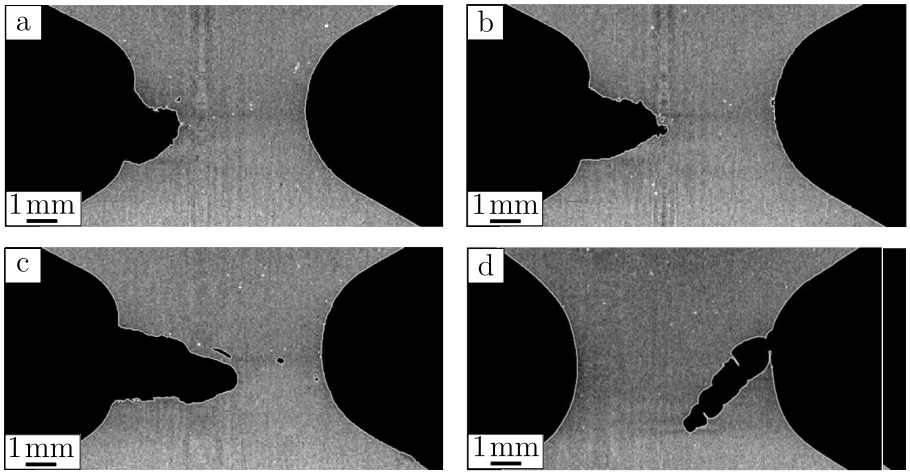

Figure 6: Propagation of the crack at right angle to the tensile direction (a-b-c) or along a different direction (d).

Still, the pictures presented on figure 6 are very interesting and help to understand what the main propagation mechanism looks like. The observations made on the different samples correlate well with what has been explained in the literature based on SEM observations. The cracks start usually from a single defect that is big enough or from the coalescence of several small cavities, with preferential location near the specimen surface. Once started, the crack propagates usually at right angle to the tensile direction. The crack then meets formerly created cavities that are disturbing the crack tip orientation, even if the main propagation direction is kept unchanged. A notable exception is illustrated on figure 6d and shows that the existing cavities may guide the propagation along a different direction for fatigue tests imposing a low displacement. The rough surface usually observed by SEM observations is clearly explained here by the progressive opening of preexisting cavities, following a mechanism already proposed by Gent and Pulford [29]. Moreover, some ligaments remaining on the border of the cracks are also observed, coming from the cavities geometry and that may be explained by locally induced crystallization [7]. One important point is that we have not observed any specific porosity at the crack tip. It therefore seems that the crack is just helping the existing cavities to open until they break and that the crack does not create any new defects, as it was proposed by Tsunoda *et al.* [30]. Nevertheless, this observation

is limited by the fact we are comparing several samples and could also be induced by the size of the smallest defect we can detect. No conical shaped cracks were observed in our samples, as related recently for filled NR and non relaxing loading conditions [8] and explained as a consequence of strain induced crystallization. This observation seems coherent with the fact that CR is less able to crystallize than NR and a null displacement ratio was imposed in order to avoid any cumulated crystallization.

2.2. Dependency of the features of the cavities population on the maximum local strain and on the number of cycles

The goal is here to relate the X-ray CT measurements to a local state of stress and strain. The material was therefore tested by the mean of standard tensile, compression and pure shear tests. The experimental data were used to identify a constitutive law and to achieve finite elements simulation of the AE2 samples, computed for the displacements imposed during the fatigue campaign. The parameters of the Mooney-Rivlin law used here were $C_1 = 0.34$, $C_2 = 0.058$ and $D = 0.000761$. As expected, the evolution of mechanical values for such sample geometry, usually used for tension-torsion testing, is complex. The best approach would therefore be to relate the observed defects to several specific zones of the measured specimen and exhibiting a nearly constant mechanical value (either strain, stress, elastic or dissipated energy for example). Still, this task requires both some numerical development and experimental validation and is scheduled as a middle term perspective. As a first evaluation, the maximum local deformation encountered in several volumes of interest will be used in the following. The choice of the maximum local strain was guided by the fact it is a classic initiation criterion [31, 32] and because the tests were displacement controlled. The use of a maximum stress criterion would lead to the same ratio between the core and the skin (about 3). The maximum value was chosen as it seemed to be the more representative of initiation, which was in most of the cases detected on the skin of the specimens. The volumes considered are defined as several slices (that will be referenced as Si in the following, see figure 7).

Except for the central slice, the data of the defect populations used in the following are the average of the values measured on symmetrical slices (S2 and S2' for example). This protocol was chosen for its simplicity and because the defect populations seemed to show no clear dependency on the radial position (as illustrated by the figure 4 for example).

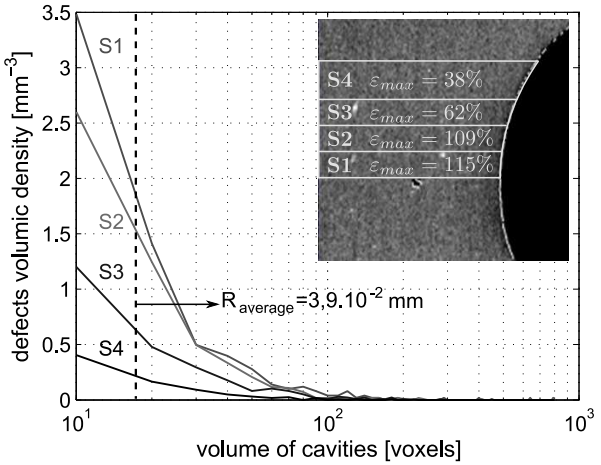

Figure 7: Comparison of the defect volumic density population of the four studied slices (referenced S1 to S4).

2.2.1. Defect population description

The obtained data are very rich and will obviously call further analysis (repartition of the defects depending on the distance to the skin, evaluation of the process influence, variation of the aspect ratio of the critical defects, etc.). In this paper, we aim at giving a first analysis based on classical features. For each samples, a statistical study was led on the defect populations. As the slices considered are not of the same volume, the volumic density of defects, *i.e.* the number of defects divided by the analyzed volume, is followed rather than the number of defects. Figure 7 shows an example of the results obtained for a sample submitted to fatigue loading (0-6 mm displacement under 2 Hz during 650 cycles, *i.e.* 10% of Ni). This description of the defect populations is useful to quickly evaluate their shape but makes the comparison between several samples difficult. This is the reason why, for each slice of each sample, we will focus on 4 parameters : the average radius of a sphere, which volume is calculated as the average volume of the defects population; the defect volumic density, *i.e.* the number of defects in a slice, divided by the volume of the slice; the porosity, calculated as the ratio between the sum of the cavity volume in a slice and the volume of the slice; the maximum size of a defect (given in mm^3) encountered in the slice. What should also be pointed out is that all the samples were obtained from the same batch. They therefore should exhibit the same initial average population of inclusions and agglomerates. Moreover, as the

samples were stretched up to the same displacement during the X-ray CT, this is not disturbing the evaluation of the defect sizes. In some cases, the samples presented some clear cracks. The defects features were then evaluated from (and rated to) the remaining not cracked volume. The critical zone is therefore ignored but this still gives a good evaluation of the defects encountered in the sample. The choice of the local maximum strain is there again enforced as it depends much less on the remaining tested section than stress, as the tests were displacement controlled.

2.2.2. Population features dependency on elongation and number of cycles

The size of the paper prevented from including the data tables (which can be supplied by the corresponding author), and in the following the analysis will be based on the charts from figures 8, 9 and 10. Figure 8 is

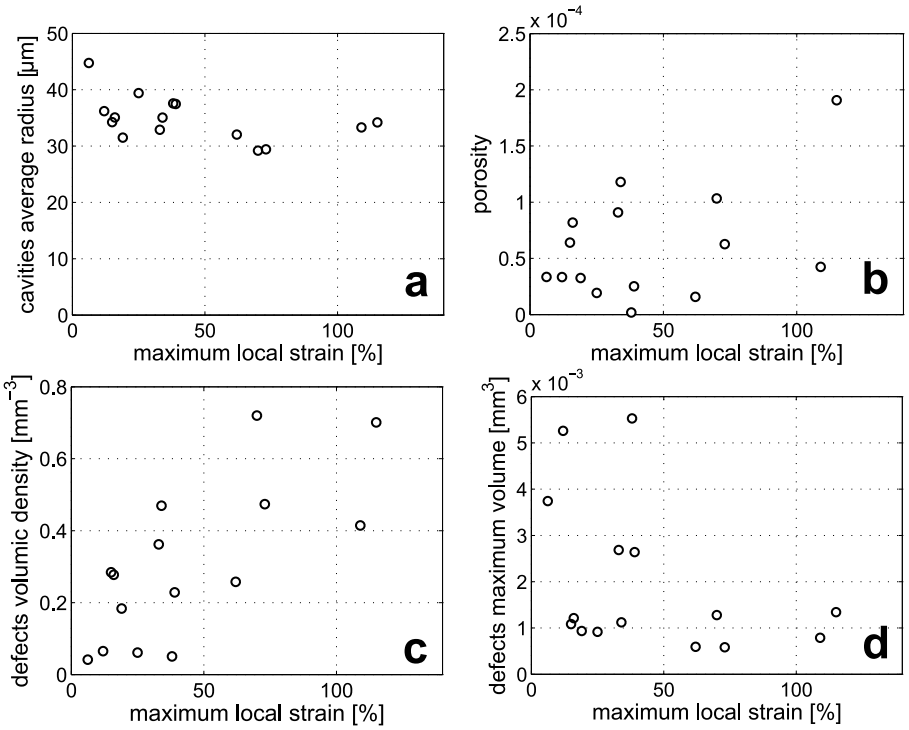

Figure 8: Evolution of the average radius of the cavities (a), the porosity (b), the defect volumic density (c) and the defect maximum volume (d) as a function of the local maximum principal strain for specimen submitted to only 5 cycles.

dedicated to the tests that lasted 5 cycles (for 0-1, 0-2, 0-3, 0-4 mm ranges of displacement) and gives the evolution of the four parameters with respect

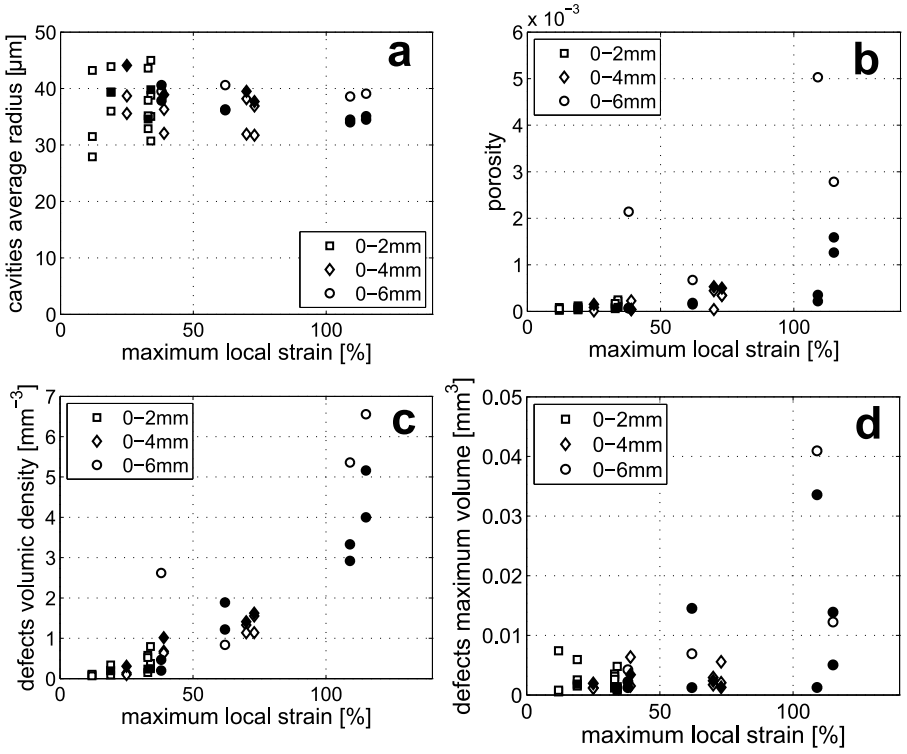

Figure 9: Evolution of the average radius of the cavities (a), the porosity (b), the defect volumic density (c) and the defect maximum volume (d) as a function of the local maximum principal strain for specimen submitted to various numbers of cycles. Filled symbols correspond to cracked samples.

to the maximum local strain. Figure 9 presents the same curves but for all the other specimens (number of cycles > 5), whatever the number of cycles imposed. Finally, Figure 10 presents the evolution of the four parameters with respect to the number of cycles, for all the tested samples, for the central slice S1 only, in order to be readable. If one first considers the defect volumic density, one can observe that it is strongly dependent on the maximum local strain, for a low number of cycles (figure 8c) as well as for high number of cycles (figure 9c). It is worth noting that on figure 9c, all the slices for all the tested samples are put together, showing a very good agreement for a same local maximum strain. It also evolves along the fatigue cycles but after a fast evolution period, it seems to saturate and to grow at a lower rate, for all the imposed displacements (figure 10c). A logarithmic scale is used here to be able to compare all the results but this observation is even clearer for non-logarithmic scaled plots and is confirmed on the other

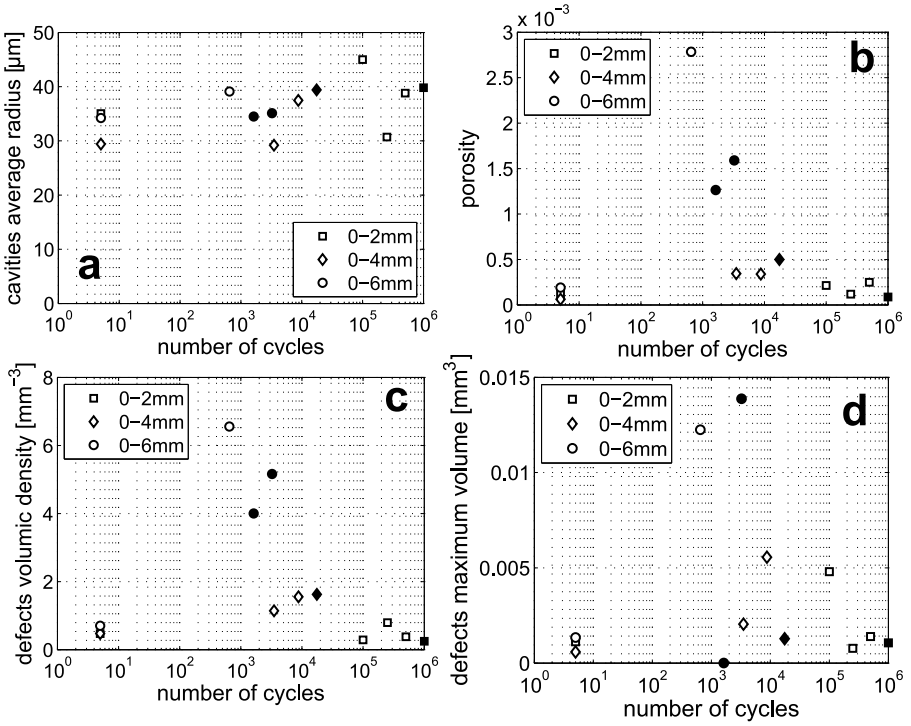

Figure 10: Evolution of the average radius of the cavities (a), the porosity (b), the defect volumic density (c) and the defect maximum volume (d) as a function of the number of cycles for the slice S1 only. Filled symbols correspond to cracked samples.

slices (only S1 is shown on figure 10c), as illustrated on figure 11 for the slices of the samples submitted to a displacement of 4 mm. Dealing with the average defect radius, it can be observed that it is not much dependent on the local strain encountered, neither for a limited number of cycles (figure 8a) nor for a high number of cycles (figure 9a) and that it increases slowly with the number of cycles (figure 10a). The average radius observed after 5 cycles is close to the one observed several decades of cycles later (average rise of 15%). The values obtained are closed from the ones observed in the literature [5, 7, 8]. It also seems that increasing the elongation reduces the dispersion observed between the different samples. This last observation is only a consequence of the averaged nature of that parameter : as the defects are less numerous for low elongations, large sized cavities have a higher influence. The fact that the average radius remains nearly constant means that the size distribution keeps the same shape (see figure 7 for example). This also means that one can not conclude, from a first sight

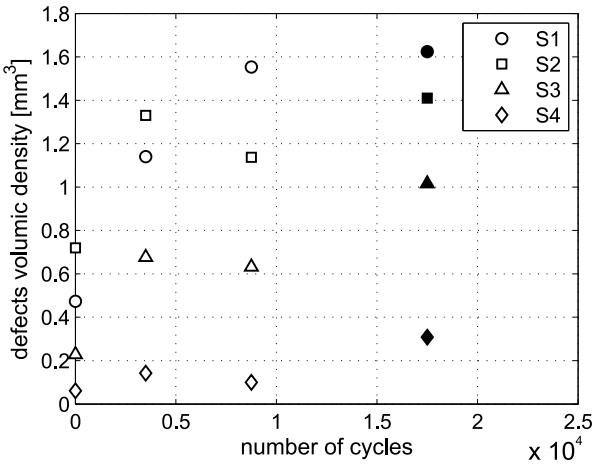

Figure 11: Evolution of the defects volumic density with respect to the number of cycles of the different slices for a displacement of 4 mm. Filled symbols correspond to cracked samples.

analysis, that the equivalent radius of the cavities is not evolving along the fatigue cycles because in a sample presenting numerous defects, the growth, even important, of a few of them will not influence much the average radius. As the same cavities are not followed from a number of cycles to another, the answers about the growth of the cavities are not as clear as for defects initiation. Still some observations on the growth of the cavities can already be done from the existing measurements.

The comparison of figures 8d and 10d shows that the maximum volume encountered changes a lot. This growth occurs mainly during the first 10% of the initiation lifetime and the growth rates of these big defects are clearly very dependant on the global displacement or maximum local elongation. Figure 10a shows that the average radius is almost the same after 5 cycles or after 10% of the initiation lifetime, with a very much lower number of defects. It means that the average size of the created defects is not evolving much and that the size repartition keeps the same shape. Between 10% and 50%, the average radius is slowly increasing, with stabilized values of the defect volumic density and of the maximum defect volume.

The evolution of the porosity is related both to the number and to the size of the defects and the logical induced evolutions are observed on figures 8b, 9b and 10b. Thus, it seems that the porosity is less sensible to the maximum size than to the number of defects. This conclusion can be

drawn for a low number of cycles (comparison of figures 8b, 8c and 8d) as well as for a high number of cycles (comparison of figures 9b, 9c and 9d).

3. Discussion

3.1. Discussion on the evolution of the population along the fatigue tests

The results presented in section 2 first confirm the initiation mechanisms observed from SEM observations. Some specific comments can be pointed out such as the high proportion of cavities initiated between close inclusions, whatever their nature and the fact that the defect volumic density does not seem to be higher at the crack tip, even if the existing cavities are opened wider. Some defects are created very early during the fatigue tests: 5 cycles are enough to initiate them, but they do not propagate yet. A clear dependency of the number of defects initiated on the global displacement (and on the local maximum strain) is observed. During the following step of the fatigue tests (until 10% of the initiation lifetime), three main observations can be done : the maximum size encountered drastically increased showing an important growth of some big cavities, the number of defects also increases very much and the average radius remains the same. This first step can therefore be considered as a fast growing period for a few defects, but also as an initiation period for the cavity populations, with only a slow growth, if any, of the large majority of the defects. These results are correlating the observations from SEM observations [26] and for X-ray CT measurements on interrupted fatigue tested specimen [8].

It therefore seems that the number of activated defects in a volume strongly depends on the experienced local strain and reaches a nearly stabilized value in a number of cycles lower than 10% of the initiation lifetime. The growth rates of the big defects as well as the rate of initiation are strongly dependant on the maximum local strain and the dependency of the defects volumic density on this local value is clearly established for different slices taken from different samples. After that first step, the average radius grows slowly, with stabilized values of the defect volumic density and of the maximum volume. It can be concluded that between 10% and 50% of the initiation time (as some samples already present some cracks, it is even 100%), the defects are slowly growing, until a local macro-crack appears. There again, clear conclusions on the growth history of the cavities will be only accessible by following a single sample submitted to several interrupted tests, which is to be done in our next investigations by going on with the already interrupted samples tested in this study. Still, a global coalescence

is not probable to happen during 50% of the initiation time as no drop of the defect volumic density is observed and because the increase of the average radius remains small: coalescence would in the same time reduces the number of defects and increases their size, and the rise of the average radius along the fatigue cycles would have been much clearer. These observations consequently confirm that coalescence of the defects is occurring very lately [8].

3.2. Discussion on some simple initiation criteria

The number of fatigue cycles leading to "initiation" is usually the one used to design massive samples (for thin samples like H2 specimens, the break follows the initiation almost immediately). From a macroscopic point of view, this number of fatigue cycles could be classically identified either as the one leading to an observable crack of 1 to 2 mm on the skin of the sample [33, 34], either as the one leading to a sudden drop of the sample stiffness [25, 34]. From X-ray CT measurements, it is clear that these criteria are limited because enormous inside cavities can be seen, very likely created before the external crack and not associated with a major drop of stiffness, as they did not appear in the thinner zone.

In this paragraph, some local initiation criteria are compared to the measurements achieved. As the values presented here are averaged on a given volume, they can not be representative of local situations leading to the creation of cavity, and illustrated in paragraph 3.1.a. Nevertheless, we may draw some conclusions. The initiation criteria based on the idea of a critical void ratio is to be excluded because the porosity and the defect volumic density measured for the different testing conditions are very different but are all leading to the appearance of a macroscopic crack. As the defect maximum size is also very different for various global displacements, one could also be tempted to exclude it as well but a single crack might propagate at a very high growth rate [35], preventing the others to grow [36], which might finally explain the discrepancy in the maximum volumes observed. From these observations, it seems to us that more convincing criteria could be based on the dissipated energy summed along the fatigue test, either as a global criterion or as a local indicator of the matrix dissipation [32, 33, 36, 37]. Here, the (low) evolution of the defect density along the fatigue cycles is measured, and so is its dependency on the global displacement or on averaged mechanical local values. The only data missing to apply a global energetic criterion would be to evaluate the energy dissipated by each defect. Finite element simulations could be achieved in

order to evaluate this energy and its dependancy on the mechanical parameters but they meet the complexity of these materials (shape of inclusions, visco-hyperelastic matrix, low compressible behaviour, difficulty to identify the interphase behaviour, etc.). In another fold of our study, a global point of view was chosen to evaluate the dissipated energy, based on the measurement of the heat build-up, which is described elsewhere [38].

Conclusions

The results presented in section 2 and discussed in section 3 first confirm the initiation mechanisms proposed from SEM observations. Two specific points can be underlined: the observation that there is no specifically high density of defects at the crack tip and the high proportion of cavities initiated between close inclusions, whatever their nature. A scenario for the evolution of the defect population can be proposed as the following. The initiations of the cavities happen very early. After only 5 cycles, the final defect density is almost reached for the fatigue tests achieved under a low displacement. Then, within a number of cycles lower than 10% of the initiation lifetime, an increase in the amount of defects is observed, with no clear increase of their volumes, except for a few of them if the specimen is submitted to high elongations. This rise of the number of cavities is strongly related to the global displacement and to the maximum local strain. After that step, the number of defects increases very slowly along the fatigue test and is coupled with an overall slow growth of the cavities. No sudden coalescence of the cavities seems to happen, except locally, helping the growth of a low number of defects that becomes micro-cracks, which do not affect the average radius of the global population. The rate growth of these cracks is very dependant on the global displacement, which can be related to the much higher density of defects already created. During this propagation phase, a shielding process of already created voids may happen.

The comparison of the results obtained for several global displacements shows that no global criteria can be related to a critical void ratio, as both porosity and number of defects are very different for specimens exhibiting macro-cracks. An energy based criterion seems to be the best choice, even if a critical size based criteria can not be excluded. The perspectives of this work are very numerous, ranging from validation of Finite Element simulations at a microscopic scale to experimental investigations for several load ratio variations, several kind of elastomers, etc.

Acknowledgements

The authors would like to thank the Brittany region for its financial support and all the partners involved in the FEMEM project. The authors also aknowledge G. Bourbouze (CRT Morlaix) for performing the tomography measurements. A special thank to P. Laguillaumie for his careful reading.

References

[1] I. Choi, C. Roland, Intrinsic defects and the failure properties of cis-1,4-polyisoprenes, Rubber Chemistry and Technology 69 (4) (1996) 591–599.
[2] K. Legorgu-jago, C. Bathias, Fatigue initiation and propagation in natural and synthetic rubbers, International Journal of Fatigue 24 (2002) 85–92.
[3] J. Le Cam, E. Verron, B. Huneau, L. Gornet, Micro-mechanism of fatigue crack growth: comparison between carbon black filled NR SBR, in: Constitutive model for rubber IV, Stockholm (Sweden), 115–120, 2005.
[4] N. Saintier, G. Cailletaud, R. Piques, Crack initiation and propagation under multiaxial fatigue in a natural rubber, International Journal of Fatigue 28 (2006) 61–72.
[5] J. Busfield, A. Thomas, M. Ngah, Application of fracture mechanics for the fatigue life prediction of carbon black filled elastomers, in: Constitutive Model for Rubber, Rotterdam (The Netherlands), 249–256, 1999.
[6] N. Saintier, Fatigue multiaxiale dans un élastomère de type NR chargé : mécanismes d'endommagement et critère local d'amorçage de fissure, Ph.D. thesis, Ecole Nationale Supérieure des Mines de Paris, 2001.
[7] J. Le Cam, B. Huneau, E. Verron, L. Gornet, Mechanism of fatigue crack growth in carbon black filled rubber, Macromolecules 37 (2004) 5011–5017.
[8] K. Le Gorgu Jago, Fatigue life of rubber components: 3D damage evolution from X-ray computed microtomography, in: Constitutive Model for Rubber V, Paris (France), 173–177, 2007.
[9] L. Salvo, P. Cloetens, E. Maire, S. Zabler, J. Blandin, J. Buffière, W. Ludwig, E. Boller, D. Bellet, C. Josserond, X-ray micro-tomography: an attractive characterisation technique in materials science, Nuclear Instrumentation and Methods in Physics Research B 200 (2003) 273–286.
[10] K. Khor, J. Buffière, W. Ludwig, H. Ubhi, P. Gregson, I. Sinclair, In situ high resolution synchrotron X-ray tomography of fatigue crack closure micromechanisms, Journal of Physics, Condensed Matter 16 (2004) 3511–3515.
[11] A. Moffat, B. Mellor, I. Sinclair, P. Reed, The mechanisms of long fatigue crack growth behaviour in Al-Si casting alloys at room and elevated temperature, Materials Science and Technology 23 (12) (2007) 1396–1401.
[12] J. Buffière, S. Savelli, P. Jouneau, E. Maire, R. Fougieres, Experimental study of porosity and its relation to fatigue mechanisms of a model Al-Si7-Mg0.3 cast Al alloy, Materials Science and Engineering A 316 (2001) 115–126.
[13] R. Hamilton, D. See, S. Butler, P. Lee, Multiscale modeling for the prediction of casting defects in investment cast aluminum alloys, Materials Science and Engineering A 343 (2003) 290–300.

[14] E. Ferrié, J. Buffière, W. Ludwig, A. Gravouil, L. Edwards, Fatigue crack propagation: In situ visualization using X-ray microtomography and 3D simulation using the extended finite element method, Acta Materialia 54 (4) (2006) 1111–1122.
[15] M. Horstemeyer, K. Gall, K. Dolan, A. Waters, J. Haskins, D. Perkins, A. Gokhale, M. Dighe, Numerical, experimental, nondestructive, and image analyses of damage progression in cast A356 aluminum notch tensile bars, Theoretical and Applied Fracture Mechanics 39 (2003) 23–45.
[16] S. Persson, How computed X-ray tomography can be used to study crosslink density in non-filled peroxide cured polyisoprene rubber, Polymer 29 (1988) 802–807.
[17] B. Mattson, B. Stenberg, S. Persson, E. Oestman, Thermo-oxidative degradation of thick-walled rubber materials studied by IR-technique and computed X-ray tomography scanning, Rubber Chemistry and Technology 63 (1990) 23–31.
[18] E. Bayraktar, F. Montembault, C. Bathias, Multiscale observation of polymer materials in order to explain mechanical behaviour and damage mechanism by X-ray computed tomography, Journal of Materials Science and Technology 20 (2004) 27–31.
[19] E. Bayraktar, S. Antolonovich, C. Bathias, Multiscale study of fatigue behaviour of composite materials by X-ray computed tomography, International Journal of Fatigue 28 (2006) 1322–1333.
[20] E. Bayraktar, S. Antolonovich, C. Bathias, New developments in non-destructive controls of the composite materials and applications in manufacturing engineering, Journal of Materials Processing Technology 206 (2008) 30–44.
[21] H. Greensmith, Rupture of rubber. X. The change in stored energy on making a small cut in a test piece held in simple extension, Journal of Applied Polymer Science 7 (1963) 993–1002.
[22] A. Gent, P. Lindley, A. Thomas, Cut growth and fatigue of rubbers. I. The relationship between cut growth and fatigue, Journal of Applied Polymer Science 8 (1964) 455–466.
[23] G. Lake, P. Lindley, The mechanical fatigue limit for rubber, Journal of Applied Polymer Science 9 (1965) 1233–1251.
[24] A. Moffat, P. Wright, J. Buffière, I. Sinclair, S. Spearing, Micromechanisms of damage in 0° splits in a [90/0]s composite material using synchrotron radiation computed tomography, Scripta materialia 59 (10) (2008) 1043–1046.
[25] E. Ostoja Kuczynski, P. Charrier, E. Verron, L. Gornet, G. Marckmann, Crack initiation in filled natural rubber: experimental database and macroscopic observations, in: Constitutive Model for Rubber III, London (UK), 41–48, 2003.
[26] J. Le Cam, Endommagement en fatigue des élastomères, Ph.D. thesis, Ecole Centrale de Nantes, Université de Nantes, 2005.
[27] A. Gent, B. Park, Failure processes in elastomers at or near a rigid spherical inclusion, Journal of Materials Science 19 (6) (1984) 1947–1956.
[28] Y. Fukahori, W. Seki, Stress analysis of elastomeric materials at large extensions using the finite elements methods. II: Stress and strain distribution around rigid spherical particles, Journal of Materials Science 28 (1993) 4471–4482.
[29] A. Gent, C. Pulford, Micromechanisms of fracture in elastomers, Journal of Materials Science 19 (6) (1984) 3612–3619.
[30] K. Tsunoda, J. Busfield, C. Davies, A. Thomas, Effect of materials variables on

the tear behaviour of a non-crystallising elastomer, Journal of Materials Science 35 (2000) 5187–5198.

[31] S. Cadwell, R. Merrill, C. Sloman, F. Yost, Dynamic fatigue life of rubber, Industrial and Engineering Chemistry 12 (1940) 19–23.

[32] E. Ostoja Kuczynski, Comportement en fatigue des élastomères : application aux structures antivibratoires pour l'automobile, Ph.D. thesis, Ecole Centrale de Nantes, Université de Nantes, 2005.

[33] C. Lu, Etude du comportement mécanique et des mécanismes d'endommagement des élastomères en fatigue et en fissuration par fatigue, Ph.D. thesis, CNAM, 1991.

[34] W. Mars, A. Fatemi, A literature survey on fatigue analysis approaches for rubbers, International Journal of Fatigue 24 (2002) 949–961.

[35] P. Charrier, E. Ostoja-Kuczynski, E. Verron, G. Marckmann, L. Gornet, G. Chagnon, Theoretical and numerical limitations for the simulation of crack propagation in natural rubber components, in: Constitutive Model for Rubber III, London (UK), 3–10, 2003.

[36] W. Mars, Multiaxial fatigue of rubber, Ph.D. thesis, University of Toledo, 2001.

[37] J. Le Cam, E. Verron, B. Huneau, Description of fatigue damage in carbon black filled natural rubber, in: Constitutive model for rubber V, Paris (france), 215–220, 2007.

[38] V. Le Saux, Y. Marco, S. Calloch, C. Doudard, P. Charrier, Fast evaluation of the fatigue lifetime of elastomers based on a heat build-up protocol and micro-tomography measurements, International Journal of Fatigue 32 (2010) 1582–1590.

Bibliographie

[Ab-Malek et Stevenson 1986] K. Ab-Malek et A. Stevenson. The effect of 42 years immersion in sea-water on natural rubber. *Journal of Materials Science*, 21 : 147–154, 1986.

[Abraham *et al.* 2005] F. Abraham, T. Alshuth, et S. Jerrams. The effect of minimum stress and stress amplitude on the fatigue life of non strain crystallising elastomers. *Materials & Design*, 26 : 239–245, 2005.

[Andrieux 1996] F. Andrieux. *Sur les milieux visco-hyperélastiques endommageables*. Thèse de doctorat, Université de Technologie de Compiègne, 1996.

[Andriyana 2006] A. Andriyana. *Définition d'une nouvelle grandeur prédictive pour la durée de vie en fatigue des matériaux élastomères*. Thèse de doctorat, Ecole Centrale de Nantes, Université de Nantes, 2006.

[Anthony *et al.* 1942] R.L. Anthony, R.H. Caston, et E. Guth. Equations of state for natural and synthetic rubber-like materials. I. Unaccelerated natural soft rubber. *The Journal of Physical Chemistry*, 46 : 826–840, 1942.

[Antunes *et al.* 2007] J.M. Antunes, J.V. Fernandes, L.F. Menezes, et B.M. Chaparro. A new approach for reverse analysis in depth-sensing indentation using numerical simulation. *Acta Materialia*, 55 : 69–81, 2007.

[Antunes *et al.* 2006] J.M. Antunes, L.F. Menezes, et J.V. Fernandes. Three-dimensional numerical simulation of vickers indentation tests. *International Journal of Solids and Structures*, 43 : 784–806, 2006.

[Antunes *et al.* 2007] J.M. Antunes, L.F. Menezes, et J.V. Fernandes. Influence of vickers tip imperfection on depth sensing indentation tests. *International Journal of Solids and Structures*, 22 : 2732–2747, 2007.

[Arruda et Boyce 1993] E.M. Arruda et M.C. Boyce. A three-dimensional constitutive model for the large stretch behavior of rubber elastic materials. *Journal of Mechanics and Physics of Solids*, 41(2) : 389–412, 1993.

[Bathias et Baïlon 1997] C. Bathias et J.-P. Baïlon. *La fatigue des matériaux et des structures (seconde édition)*. Hermès, 1997.

[Bayraktar *et al.* 2006] E. Bayraktar, S. Antolonovich, et C. Bathias. Multiscale study of fatigue behaviour of composite materials by X-ray computed tomography. *International Journal of Fatigue*, 28 : 1322–1333, 2006.

[Beatty 1964] J.R. Beatty. Fatigue of rubber. *Rubber Chemistry and Technology*, 37(5) : 1341–1364, 1964.

[Belytschko *et al.* 2000] T. Belytschko, W.K. Liu, et B. Moran. *Nonlinear finite elements for continua and structures*. Wiley, 2000.

[Bennani 2006] A. Bennani. *Elaboration, comportement et durée de vie du caoutchouc naturel renforcé de silice*. Thèse de doctorat, Ecole Nationale Supérieure des Mines de Paris, 2006.

[Bergström et Boyce 1998] J.S. Bergström et M.C. Boyce. Constitutive modeling of the large strain time-dependend behavior of elastomers. *Journal of the Mechanics and Physics of Solids*, 46 : 931–954, 1998.

[Bernstein *et al.* 1963] B. Bernstein, E.A. Kearsley, et L.J. Zapas. A study of stress relaxation with finite strain. *Transaction of the Society of Rheology*, 7 : 391–410, 1963.

[Bernstein *et al.* 2005] R. Bernstein, D.K. Derzon, et K.T. Gillen. Nylon 6.6 accelerated ageing studies : thermal-oxydative degradation and its interaction with hydrolysis. *Polymer Degradation and Stability*, 480-488 : 80, 2005.

[Bolland et Gee 1946] J.L. Bolland et G. Gee. Kinetic studies in the chemistry of rubber and related materials. II. The kinetics of oxydation in unconjugated olefins. *Transactions of the Faraday Society*, 42 : 236–243, 1946.

[Bonet 2001] J. Bonet. Large stain viscoelastic constitutive models. *International Journal of Solids and Structures*, 38 : 2953–2968, 2001.

[Bonet et Wood 1997] J. Bonet et R.D. Wood. *Nonlinear continuum mechanics for finite element analysis*. Cambridge University Press, 1997.

[Bouasse et Carrière 1903] H. Bouasse et Z. Carrière. Sur les courbes de traction du caoutchouc vulcanisé. *Annales de la Faculté des Sciences de Toulouse 2^e série*, 5(3) : 257–283, 1903.

[Boulanger *et al.* 2004] T. Boulanger, A. Chrysochoos, C. Mabru, et A. Galtier. Calorimetric analysis of dissipative and thermoelastic effects associated with the fatigue behavior of steels. *International Journal of Fatigue*, 26 : 221–229, 2004.

[Bowditch et Stannard 1985] M.R. Bowditch et K.J. Stannard. Effects of water absorption on the properties of a filled elastomer. Dans *Polymers in Marine Environments*, pages 117–119, London (Great-Britain), October 31th - November 2nd 1985.

[Brown et Soulagnet 2001] R.P. Brown et G. Soulagnet. Microhardness profiles on aged rubber compounds. *Polymer testing*, 20 : 295–303, 2001.

[Bucaille 2001] J.L. Bucaille. *Simulation numérique de l'indentation et de la rayure des verres organiques*. Thèse de doctorat, Ecole Nationale Supérieure des Mines de Paris, 2001.

[Budrugeac et Ciutacu 1991] P. Budrugeac et S. Ciutacu. Thermal degradation of polychloroprene rubber. *Polymer Degradation and Stability*, 33 : 377–386, 1991.

[Buffière *et al.* 2001] J.Y. Buffière, S. Savelli, P.H. Jouneau, E. Maire, et R. Fougères. Experimental study of porosity and its relation to fatigue mechanisms of a model Al-Si7-Mg0.3 cast Al alloys. *Materials Science and Engineering A*, 316 : 115–126, 2001.

[Cadwell *et al.* 1940] S.M. Cadwell, R.A. Merrill, C.M. Sloman, et F.L. Yost. Dynamic fatigue life of rubber. *Industrial and Engineering Chemistry*, 12(1) : 19–23, 1940.

[Caston 1942] R.H. Caston. *Equation of state of rubber*. Thèse de doctorat, University of Notre Dame, 1942.

[Cazaud 1959] R. Cazaud. *La fatigue des métaux*. Dunod, Paris (France), 1959.

[Celina *et al.* 2005] M. Celina, K.T. Gillen, et R.A. Assink. Accelerated aging and lifetime prediction : review of non-Arrhenius behaviour due to two competing processes. *Polymer Degradation and Stability*, 90 : 395–404, 2005.

[Celina *et al.* 2000] M. Celina, J. Wise, D.K. Ottesen, K.T. Gillen, et R.L. Clough. Correlation of chemical and mechanical property changes during oxydative degradation of neoprene. *Polymer Degradation and Stability*, 68 : 171–184, 2000.

[Chagnon 2004] G. Chagnon. *Modélisation de l'effet Mullins dans les élastomères*. Thèse de doctorat, Ecole Centrale de Nantes, Université de Nantes, 2004.

[Chagnon *et al.* 2004] G. Chagnon, E. Verron, L. Gornet, G. Marckmann, et P. Charrier. On the relevance of Continuum Damage Mechanics as applied to the Mullins effect in elastomers. *International Journal of the Mechanics and Physics of Solids*, 52 : 1627–1650, 2004.